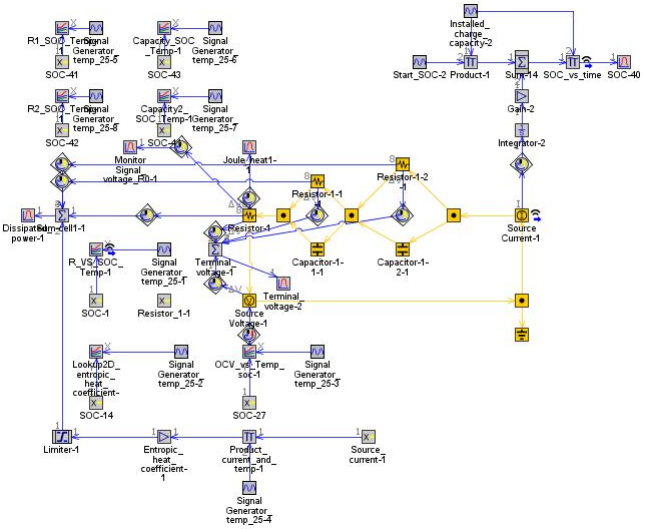
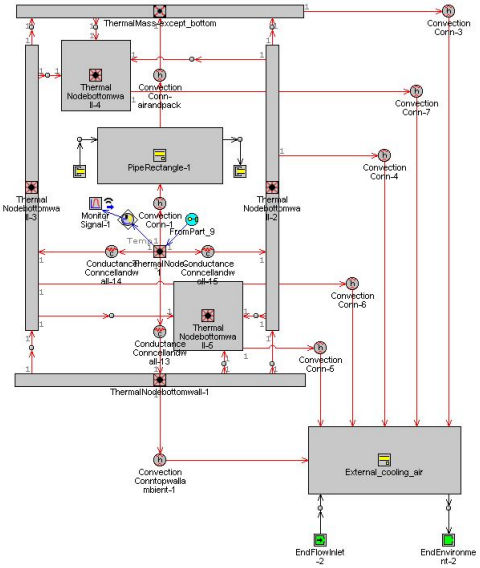
CHALMERS
UNIVERSITY OF TECHNOLOGY





Mild Hybrid Electro-Thermal Battery Modelling

Master of Science Thesis

AKIK BISWAS

XUMING YAO

Department of Energy and Environment
CHALMERS UNIVERSITY OF TECHNOLOGY
Gothenburg, Sweden 2016

Master of Science Thesis Report

Mild Hybrid Electro-Thermal Battery Modelling

AKIK BISWAS XUMING YAO



CHALMERS
UNIVERSITY OF TECHNOLOGY

Department of Energy and Environment
Division of Electric Power Engineering
Chalmers University of Technology
Gothenburg, Sweden 2016

Mild Hybrid Electro-Thermal Battery Modelling

© AKIK BISWAS and XUMING YAO, 2016.

Supervisors:
Raik C. Orbay, Volvo Cars Corporation
Patrik Stridh, Volvo Cars Corporation
Stefan Skoog, Chalmers University of Technology

Examiner: Torbjörn Thiringer, Chalmers University of Technology

Master of Science Thesis Report
Department of Energy and Environment
Division of Electric Power Engineering and Automotive Engineering
Chalmers University of Technology
SE-412 96 Gothenburg
Telephone +46 31 772 1000

Cover:

Typeset in LaTeX
Printed by [Chalmers Reproservice]
Göteborg, Sweden 2016

Mild Hybrid Electro-Thermal Battery Modelling
AKIK BISWAS and XUMING YAO
Department of Energy and Environment
Chalmers University of Technology

Abstract

In this thesis an electro-thermal battery pack model has been developed for a 48 V Mild Hybrid vehicle application to predict the pack temperature under different loading cases which have been verified with experiments.

Both the joule and the entropic heat play significant roles in the total heat generation process. Furthermore, the entropic heat can be both endothermic and exothermic and these processes have also been verified. The contribution of entropic heat to the thermal dynamic behavior was verified through simulations using GTSUITE® software and experiment. For the electrical battery pack model it was found that the 2 RC circuit model captured the electrical dynamic behavior which was in good agreement with the experiment data, whereas the 0 RC circuit model failed to do so. The 2 RC circuit model produced an error of 1.5 %, whereas the 0 RC circuit model gave an error of 3.2 %. Experiments were carried out both at the battery pack for temperature measurements and at the cell level to determine the internal battery cell parameters such as R_0, R_1, R_2, C_1, C_2, specific heat and the entropic heat. Moreover, the experiments were carried out over a wide range of state of charge (SOC) levels and temperatures restricted between 5 °C and 45 °C.

Keywords: electro-thermal, 48 V battery modelling, joule heat, entropic heat, GTSUITE®, RC circuit.

Acknowledgements

This work has been carried out at the Division of Electric Power Engineering, Department of Energy and Environment at Chalmers University of Technology, Gothenburg, Sweden and Volvo Cars Group, Gothenburg, Sweden.

We would like to express our gratitude to the following people

- our supervisors Stefan Skoog, Raik Orbay and Patrik Stridh who have been very instrumental in guiding us throughout the thesis work.
- our examiner Torbjörn Thringer for all the help with providing wonderful insights and help.
- our manager Pelle Thorson for providing us with the opportunity to conduct the thesis at Volvo Cars Group.
- special thanks to Peter Stopp from Gamma Technologies for all the help with GTSUITE®, Kristian Frenander and Sam Gullman for the help with thermal modelling, Patrik Larsson, Jonas Sjögren and Astrid Lundgren for sharing with us their battery knowledge.
- last but not the least to our friend Sandeep David for helping us out with some of the experiment measurements.

Akik and Xuming, Gothenburg, June 2016

Preface

"*Electric drive is as old as the automobile itself.....For a century though, the deal-breaker has been the* ***battery***" - Jonathan Raunch, The Atlantic

The above quote sums it all! If there is one technology which has a lot of potential for further research, it is the energy storage technology. Battery technology is the unification of chemical, electrical, thermal and mechanical disciplines. Is it not great that one can acquire a skill set from one engineering discipline and gain skill sets from other areas as well? Hence, we were both fortunate to learn from each other and participate in a cross-functional team project.

Batteries are amazing and everyone is speaking about it. Perhaps, we human beings feel more connected with things with a similar taste. Batteries get irritated at very low and very high temperatures and enjoy working around the optimal temperature range, just like us. Naturally, getting an accurate temperature prediction for the battery pack became our sole goal.

Contents

1 Introduction **1**
- 1.1 Background . . . 1
- 1.2 Aim . . . 1
- 1.3 Problem overview and our contribution . . . 1
- 1.4 Scope . . . 2

2 Theory **3**
- 2.1 Mild hybrids . . . 3
- 2.2 Battery Electro-Thermal concepts . . . 3
  - 2.2.1 Battery thermal terminology . . . 3
  - 2.2.2 Dimensionless numbers . . . 4
  - 2.2.3 Battery electrical terminology . . . 4
- 2.3 Lithium-ion batteries . . . 5
  - 2.3.1 Lithium ion cathode chemistries . . . 5
  - 2.3.2 Lithium-ion battery packaging . . . 6
  - 2.3.3 Temperature effects on lithium-ion batteries . . . 6
  - 2.3.4 Description about reversible and irreversible heat . . . 7
- 2.4 Partial differential equation of thermal model . . . 8
- 2.5 Lumped parameter method . . . 9
- 2.6 Lumped parameter method vs FEA . . . 10
- 2.7 Single cell equivalent electrical circuits . . . 11
  - 2.7.1 0 RC circuit model . . . 11
  - 2.7.2 2 RC circuit model . . . 11

3 Case Setup **13**
- 3.1 Description of the cell and the battery pack . . . 13
- 3.2 General description of the Electro-Thermal Battery Model . . . 15
- 3.3 Convection coefficient determination . . . 16
  - 3.3.1 Free Convection . . . 16
  - 3.3.2 Forced Convection . . . 17
- 3.4 Contact conductance . . . 17
- 3.5 Single cell electro-thermal model using GT-SUITE® . . . 20
  - 3.5.1 Single cell electrical model . . . 20
  - 3.5.2 Single cell thermal model . . . 21

4 Experiment **25**

4.1 48 V battery pack experiments . . . 25
4.1.1 Application of a constant current to the battery pack . . . 25
4.1.1.1 Purpose . . . 25
4.1.1.2 Procedure . . . 25
4.1.2 Application of a charge-discharge current to the battery pack . 26
4.1.2.1 Purpose . . . 26
4.1.2.2 Procedure . . . 26
4.1.3 Test Conditions . . . 28
4.2 Experiments on a single cell attached to an aluminium cooling plate . 29
4.2.1 Purpose . . . 29
4.2.2 Experiment 1: Nominal capacity and open circuit voltage measurement . . . 29
4.2.2.1 Purpose . . . 29
4.2.2.2 Procedure . . . 29
4.2.3 Experiment 2: Cell impedance measurements . . . 31
4.2.3.1 Purpose . . . 31
4.2.3.2 Procedure . . . 31
4.2.4 Experiment 3: Determination of the specific heat C_p value . . 32
4.2.4.1 Purpose . . . 32
4.2.4.2 Procedure . . . 32
4.2.5 Risk Analysis . . . 33

5 Results **35**
5.1 Experiment results . . . 35
5.1.1 Cell capacity at different temperatures for both charging and discharging . . . 35
5.1.2 Open circuit voltage as a function of SOC and temperature . . 36
5.1.3 Entropic heat coefficient depending on SOC and temperature . 37
5.1.4 Cell impedance measurements . . . 38
5.1.5 Verification of the entropic heat . . . 44
5.2 Sensitivity analysis of the battery pack thermal model . . . 45
5.2.1 Contact pressure between the cell and the cooling plate . . . 45
5.2.2 Air gap between cell and cell . . . 46
5.2.3 Volumetric velocity of cooling air . . . 47
5.2.4 Thermal time constant . . . 48
5.3 Comparison between the experiment and the simulation results . . . 50
5.3.1 Terminal voltage comparison between the simulation prediction and the experiment . . . 50
5.3.2 Temperature comparison between the simulation model and the experiment . . . 55
5.4 Simulation with the WLTP driving cycle . . . 58

6 Conclusions **61**
6.1 Conclusions . . . 61
6.2 Discussions . . . 61
6.3 Future work . . . 62

Bibliography **63**

Abbreviations

ICE ..... Internal Combustion Engine
EV ..... Electric Vehicle
HEV ..... Hybrid Electric Vehicle
NMC ..... Lithium Nickel Manganese Cobalt Oxide
NCA ..... Lithium Nickel Cobalt Aluminum Oxide
LMO ..... Lithium Manganese Oxide
LTO ..... Lithium Titanate
LFP ..... Lithium Iron Phosphate
FEA ..... Finite Element Analysis
RAM ..... Random Access Memory
LiPF6 ..... Lithium Hexafluorophosphate
SOC ..... State of Charge
SEI ..... Solid Electrolyte Interphase
EC ..... Ethylene Carbonate
EMC ..... Ethyl Methyl Carbonate
CPU ..... Central Processing Unit
WLTP ..... Worldwide Harmonized Light Vehicles Test Procedure

Nomenclature

Symbol	Units	Description
q_{cond}	W	Conductive heat transfer rate
k	W/mK	Thermal conductivity
A	m^2	Cross section area
$\frac{dT}{dx}$	K/m	Temperature gradient
q_{conv}	W	Convective heat transfer rate
h	W/m^2K	Convection heat transfer coefficient
T_s	K	Surface temperature
T_∞	K	Fluid temperature
Gr	–	Grashof number
g	m/s^2	Gravitational acceleration
β	1/K	Coefficient of volumetric expansion
L	m	Characteristic length
ν	m^2/s	Kinematic viscosity of the fluid
Re	–	Reynolds number
v	m/s	Fluid flow velocity
Pr	–	Prandtl number
α	m^2/s	Thermal diffusivity of the fluid
ρ	kg/m^3	Density
C_p	J/kgK	Specific heat
T	K	Temperature
Bi	–	Biot number
V	m^3	Battery cell volume
Nu	–	Nusselt number
h_j	W/m^2K	Thermal joint conductance per unit area
h_c	W/m^2K	Thermal contact conductance per unit area
h_g	W/m^2K	Thermal gap conductance per unit area
k_s	W/mK	Effective thermal conductivity
m_s	–	Effective mean absolute surface slope
σ_s	m	Effective RMS surface roughness
P	Pa	Pressure
H_c	Pa	Surface microhardness
k_s	W/mK	Effective thermal conductivity
m_s	–	Effective mean absolute surface slope
σ	m	RMS surface roughness
M	m	Gas parameter
Y	m	Effective gap thickness
R_{th}	K/W	Thermal resistance
C_{th}	J/K	Total heat capacity
δ	m	Gap thickness
τ	s	Thermal time constant

1
Introduction

1.1 Background

Due to growing concerns over petroleum supplies and air pollution, electric vehicles including hybrid electric vehicles are being developed and refined as cost-effective, reliable and safe alternatives to conventional gasoline and diesel engines [1].

Energy storage devices are one of the key elements in hybrid vehicles which provide power assist to the internal combustion engine, thereby enabling manufactures to downsize the engine. A smaller ICE improves the efficiency of the powertrain system and reduces emissions and fuel consumption [2].

Since the cost and reliability of the vehicle depend upon the battery pack cost, durability and life cycle, any parameter that affects the battery pack has to be optimized. *Temperature range* and *pack temperature uniformity* are important factors for obtaining optimum performance from an EV or HEV battery pack [3].

1.2 Aim

The aim of the thesis is to develop an electro-thermal battery pack model, which can estimate the battery temperature under certain loading cases. Experiments have been carried out to determine the battery pack temperature under certain loading cases in order to verify the simulation model and also to extract the battery cell parameters, such as the charging and discharging capacities under different temperatures, the open circuit voltage and the internal cell impedance depending on the SOC and the temperature.

1.3 Problem overview and our contribution

In vehicle applications, the batteries are subjected to intensive operating cycles thereby producing high Joule heating losses which increases the battery operating temperature. High temperature accelerates battery aging and might lead to a thermal runaway condition, whereas low temperature could lead to dendrite growth, thereby affecting the battery performance [6].

Our work focuses on the temperature prediction for a 48 V lithium-ion battery pack from Volvo Cars Group. We have investigated the heating effects on the battery

pack by taking into account both the joule losses and the entropic heat. Experiments were conducted both at the cell and at the pack level.

1.4 Scope

The following points have been investigated:

- The role of both joule and entropic heat on the total heat dissipation from the battery pack and their influence on the battery pack temperature.
- The role of 2 RC circuits instead of 0 RC circuit and the effect on the model accuracy.

The following points have not been investigated:

- We have not investigated the effects of temperature extremes on the battery operation, but detailed studies have been conducted by Pesaran and Santhanagopalan [6]. The reason for neglecting the temperature extremes is because according to [40] the battery would be used in the optimum temperature ranges.
- The radiation effects of the battery pack have been neglected, because the battery won't be operated under thermal runaway conditions according to [40]. According to Dan [5], the typical thermal runaway temperature for lithium ion cells varies from 130 $°C$ to well over 200 $°C$.
- Only the temperature simulation result for a driving cycle has been obtained and verification of the driving cycle case in real-time has not been considered due to time constraints, but it has been proposed as a future work.

2
Theory

In the following chapter, we have described the background theory involved in the thesis work. We begin with a brief theoretical description about the thesis title and then proceed with explaining the reasoning behind each term.

2.1 Mild hybrids

A Mild hybrid can be defined as a conventional internal combustion engine (ICE) vehicle with an oversized starter motor that can also be used as a generator, usually called an integrated starter-generator (ISG), and an oversized battery that powers and is recharged by the motor [7]. In a Mild hybrid, there is no engine shutdown when the vehicle is moving [7]. However, when the vehicle is idle the motor/generator can be used to enable idle stop in which the engine is turned off [7]. The motor/generator can be used at high loads to assist the engine and increase vehicle performance and at low loads, it increases load on the engine and recharges the electric battery [7].

2.2 Battery Electro-Thermal concepts

2.2.1 Battery thermal terminology

- Conduction - It is a heat transfer process which occurs when a temperature gradient exists in a stationary medium which may be a solid or a fluid as suggested in [8]. The equation quantifying conduction is

$$q_{cond} = -kA\frac{dT}{dx} \tag{2.1}$$

  where q_{cond} is the conductive heat transfer rate, k is the thermal conductivity, dT is the temperature difference and dx is the length and A is the cross -section area across which the conduction phenomenon takes place.
- Convection - It is a heat transfer process which occurs between a surface and a moving fluid when they are at different temperatures as suggested in [8]. The equation quantifying convection is

$$q_{conv} = hA(T_s - T_\infty) \tag{2.2}$$

  where, q_{conv} is the convective heat transfer rate, h is the convection heat transfer coefficient, T_s is the surface temperature, T_∞ is the fluid temperature and A is the cross-section area across which there is convection.

2.2.2 Dimensionless numbers

Dimensionless numbers are used to characterize and classify heat transfer problems.

Below is a list of the dimensionless numbers used in the thesis.

- Grashof number - The Grashof number is a measure of the ratio of the buoyancy forces to the viscous forces acting on the fluid. It is used for analyzing the fluid velocity distributions in free or natural convection and it is expressed as in [8]

$$Gr = \frac{g\beta(T_s - T_\infty)L^3}{\nu^2} \tag{2.3}$$

  where Gr is the Grashof number, g is the gravitational acceleration, β is the coefficient of volumetric expansion of a fluid, T_s is the surface temperature, T_∞ is the fluid temperature, L is the characteristic length of the geometry and ν is the kinematic viscosity of the fluid.
- Reynolds number - It is a measure of the ratio of the inertial to the viscous forces acting on the fluid element and it is expressed as in [8]

$$Re = \frac{vL}{\nu} \tag{2.4}$$

  where v is the fluid flow velocity, ν is the kinematic viscosity and L is the characteristic length of the geometry.
- Prandtl number - It is the ratio of the kinematic viscosity to the thermal diffusivity of the fluid and it is expressed as in [8]

$$Pr = \frac{\nu}{\alpha} \tag{2.5}$$

  where ν is the kinematic viscosity of the fluid and α is the thermal diffusivity of the fluid.

2.2.3 Battery electrical terminology

Below is a list of the electrical terminology associated with the battery and used in the thesis.

- State of Charge (SOC) - It is used to express the current battery capacity as a percentage of the maximum capacity. It is calculated using current integration to determine the change in battery capacity over time [9].
- Depth of Discharge (DOD) - The percentage of battery capacity that has been discharged expressed as a percentage of maximum capacity [9].
- Terminal Voltage - It is the voltage between the battery terminals with load applied. The terminal voltage varies with SOC and discharge/charge current [9].
- Open-circuit voltage (OCV) - It is the voltage between the battery terminals with no load applied and it depends upon the battery state of charge, increasing with it [9].
- Cut-off voltage - It is the minimum allowable voltage, which defines the 'empty' state of the battery [9].

- Nominal capacity - It is a measure of the charge, i.e the total amp-hours available when the battery is discharged from say 100 % SOC to the cut-off voltage [9].
- C-rate - It is a measure of the rate at which a battery is discharged relative to its maximum capacity. For example, a 1C-rate means that the discharge current will discharge the entire battery in 1 hour [9].

2.3 Lithium-ion batteries

2.3.1 Lithium ion cathode chemistries

Table 2.1 depicts the various lithium-ion chemistries. However, there is no single chemistry which meets all the requirements. The main motivation to include this section is because

Table 2.1: Tradeoffs between the various lithium ion-cathode chemistries; 1 being the worst score and 4 being the best score. Data has been adapted from [18].

	Cost	Specific Power	Specific Energy	Safety	Performance	Life span
NCA	2	4	4	2	3	4
NMC	3	3	4	3	3	3
LMO	3	3	3	3	2	2
LTO	1	3	2	4	4	4
LFP	3	3	2	4	3	4

From Table 2.1, we can see that the chemistries NCA, NMC and LMO have high specific energy and the chemistries LTO and LFP score high in safety. The best chemistry is the one having a high score in all the indices. Below are the five key performance parameters.

- Safety - It is the most important parameter for hybrid or electric car batteries. Avoiding thermal runaway conditions, due to an overcharged battery, very high discharge rates, or a short circuit is the main goal. By providing system-level safety measures such as having a robust battery box, an efficient cooling system, precise state-of-charge monitoring and cell-discharge balancing, the battery can be made more safer for less safe cathode chemistries such as NCA, NMC and LMO [18].
- Life Span - Battery life span is measured in two ways: cycle life and calendar life. Cycle life is expressed as the number of charge and discharge cycles that can be achieved depending to what level the battery is discharged - its 'depth of discharge'. For a fixed temperature as the DOD increases or as the SOC decreases, the cycle life decreases [19].

  Calendar life is a measure of how long the battery is expected to last in terms of calendar years and it is independent of how much the battery is charged and discharged [19]. Both the SOC and the temperature have a detrimental impact on the calendar life [19].

- Performance - Batteries cannot be used over a wide temperature range and have to be optimized for either low or high temperatures. One has to compromise on performance degradation for a wide temperature window operation [18]. A solution could be to opt for climate specific batteries. For example, a battery in a cold climate needs to be heated or insulated for optimum performance, whereas a battery for hot weather operation would require electrolytes and materials which allow a high temperature storage [18]. Even though climate specific batteries possess high functionality, they hinder vehicle mobility across regions and if restrictions are removed, then the system cost would increase [18].
- Specific Energy - It is the capacity for storing energy per kilogram of weight. Battery cells can reach nominal energy densities of 140 to 170 Wh/kg compared with 13,000 Wh/kg for gasoline and the specific energy of the resulting battery pack is typically 30 to 40 percent lower, or 80 to 120 Wh/kg [18]. Specific energy is important for PHEVs and EVs, because energy translates into vehicle range and high energy is needed to provide adequate range within space and weight constraints [20].

- Specific Power - It is the amount of power that batteries can deliver per kilogram of mass. Specific power is important in hybrid vehicles, because power translates into torque and acceleration, which is needed to provide the boost in HEV applications and the ability to capture the regenerative braking energy [20, 21].

2.3.2 Lithium-ion battery packaging

Lithium ion batteries come in many packaging varieties. Here we have described the three most common types relevant to the automotive industry with a brief discussion about their advantages and disadvantages.

- Cylindrical type - This design has good cycling ability, has a long calendar life and is economical. However, it is heavy and has a lower packaging density due to space cavities. Cylindrical cells find applications in power tools, medical instruments, laptops, e-bikes and automobiles [25].
- Prismatic type - It improves space utilization and allows flexible design, but it can have a higher manufacturing costs, less efficient in thermal management and posseses a shorter cycle life than the cylindrical type and prismatic cells are mostly found in mobile phones, tablets etc [25].
- Pouch type - It offers the most efficient use of space and they achieve 90% to 95% packaging efficiency. However, they suffer from swelling which can be harmful, because the pressure created can crack the battery cover and pouch cells find applications in the consumer, military and automotive industries [25].

2.3.3 Temperature effects on lithium-ion batteries

Under cold temperature, viscosity changes in the electrolyte lead to sluggish ion transport and the polymeric components within the cell become brittle [6]. So, the

battery performance (power,energy) becomes lower.

Dendrite growth at low temperature is another problem. Dendrites form when the battery electrode degrades, and metal ions become deposited on the electrode's surface. When they penetrate the seperator between the two electrodes, electrical shorting or overheating of the battery can occur [22].

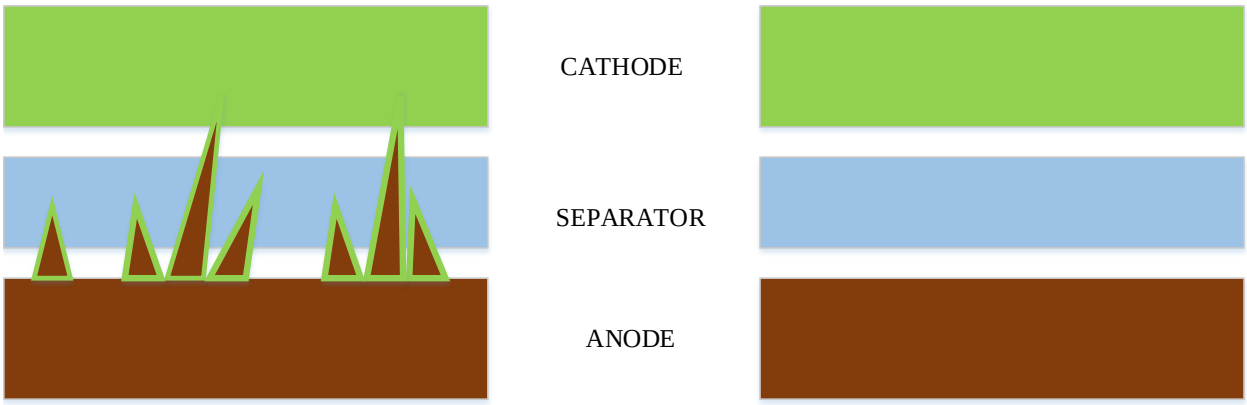


Figure 2.1: Dendrite formation adapted from [22]

Under hot temperatures, the batter degrades faster, because side reactions happen faster on the electrode surface (especially the anode), so there is a fast build-up of resistance at the electrode surface [6].

2.3.4 Description about reversible and irreversible heat

The total heat generation rate inside a cell is expressed as in [24].

$$\dot{Q} = \dot{Q}_r + \dot{Q_{irr}} \tag{2.6}$$

where $\dot{Q}_r$ is the reversible heat component and $\dot{Q_{irr}}$ is the irreversible heat component. The reversible heat generation rate, generated by a cell is expressed as in [24]

$$\dot{Q}_r = T\Delta S\frac{I}{nF} \tag{2.7}$$

where I is the current density, T is the temperature, ΔS is the entropy change, n equals the number of electrons per reaction, and F is the Faraday constant. For one Li^+ exchange during charge or discharge , the entropy change is calculated as in [24]

$$\Delta S = \frac{nF\partial U}{\partial T} \tag{2.8}$$

where U is the open circuit potential and n equals one.

In this thesis we have assumed the heat generation for exothermic reactions to be positive and the discharge current to be negative in accordance with [24]

The irreversible heat generation rate is always exothermic and is expressed as in [24].

$$\dot{Q_{irr}} = I^2 R_i \tag{2.9}$$

where R_i is the internal resistance of the cell.

2.4 Partial differential equation of thermal model

The transient 3 dimensional heat transfer equation in Cartesian coordinates inside the battery cell is described as

$$\rho C_p \frac{\partial T}{\partial t} = \frac{\partial}{\partial x}\left(k_x \frac{\partial T}{\partial x}\right) + \frac{\partial}{\partial y}\left(k_y \frac{\partial T}{\partial y}\right) + \frac{\partial}{\partial z}\left(k_z \frac{\partial T}{\partial z}\right) \tag{2.10}$$

where ρ is the density, C_p is the specific heat per unit mass, T is the cell temperature, k_x, k_y and k_z are the thermal conductivities along x,y and z directions respectively.

The heat flow into the element volume can be described as

$$d\dot{Q}_x = -k_x \delta_y \delta_z \frac{\partial T}{\partial x} \tag{2.11}$$

The heat flow out of the element volume through x=x+dx can be described by Fourier's Law as

$$\dot{dQ_{x+dx}} = d\dot{Q}_x + \frac{\partial}{\partial x} d\dot{Q}_x \delta_x \tag{2.12}$$

Then the net heat flow of each element is shown as

$$d\dot{Q}_x - \dot{dQ_{x+dx}} = \frac{\partial}{\partial x} d\dot{Q}_x \delta_x = \frac{\partial}{\partial x}(k_x \frac{\partial T}{\partial x})\delta_x \delta_y \delta_z \tag{2.13}$$

Similarly, the equations for y, z axis can be formulated as

$$d\dot{Q}_y - \dot{dQ_{y+dy}} = \frac{\partial}{\partial y} d\dot{Q}_y \delta_y = \frac{\partial}{\partial y}(k_y \frac{\partial T}{\partial y})\delta_x \delta_y \delta_z \tag{2.14}$$

$$d\dot{Q}_z - \dot{dQ_{z+dz}} = \frac{\partial}{\partial z} d\dot{Q}_z \delta_z = \frac{\partial}{\partial z}(k_z \frac{\partial T}{\partial z})\delta_x \delta_y \delta_z \tag{2.15}$$

Fig. 2.2 captures the heat flow in an elemental volume of a single cell.

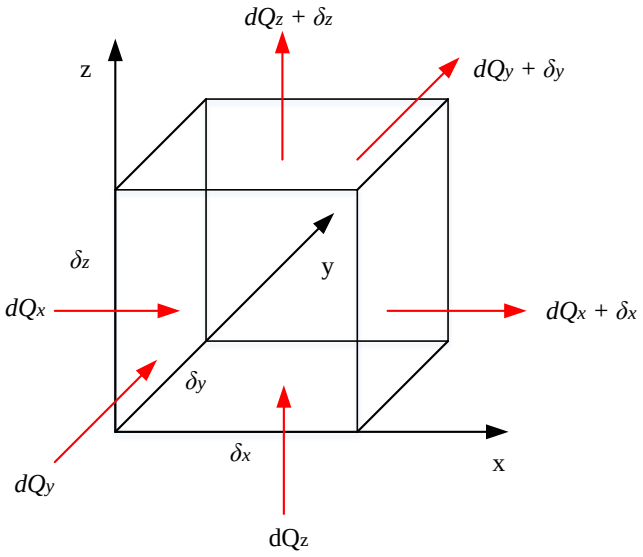


Figure 2.2: An illustration of the heat flow in an elemental volume of a single cell

The transient 3-dimensional heat transfer equation (heat flow) in Cartesian coordinates inside the cell can be described as

$$\delta_x\delta_y\delta_z\rho C_p\frac{\partial T}{\partial t} = \delta_x\delta_y\delta_z\left[\frac{\partial}{\partial x}\left(k_x\frac{\partial T}{\partial x}\right) + \frac{\partial}{\partial y}\left(k_y\frac{\partial T}{\partial z}\right) + \frac{\partial}{\partial z}\left(k_z\frac{\partial T}{\partial z}\right)\right] + \dot{Q} \quad (2.16)$$

The left side of the equation shows the rate of internal energy variation of the cell in unit time, while the first three terms on the right side are the rate of heat conduction among elements inside the cell and $\dot{Q}$ shows the total rate of heat generation. The simplified heat conduction partial differential equation is expressed as

$$\delta_x\delta_y\delta_z\rho C_p\frac{\partial T}{\partial t} = \delta_x\delta_y\delta_z\left[\frac{\partial}{\partial x}\left(k_x\frac{\partial T}{\partial x}\right) + \frac{\partial}{\partial y}\left(k_y\frac{\partial T}{\partial z}\right) + \frac{\partial}{\partial z}\left(k_z\frac{\partial T}{\partial z}\right)\right] + \dot{Q} \quad (2.17)$$

Equation (2.17) doesn't take the heat convection on the cell surface into account. If the heat convection is considered (2.17) takes the form

$$\begin{aligned} 2h(\delta_x\delta_y + \delta_y\delta_z + \delta_x\delta_z)(T - T_\infty) + \delta_x\delta_y\delta_z\rho C_p\frac{\partial T}{\partial t} = \\ \delta_x\delta_y\delta_z\left[\frac{\partial}{\partial x}\left(k_x\frac{\partial T}{\partial x}\right) + \frac{\partial}{\partial y}\left(k_y\frac{\partial T}{\partial z}\right) + \frac{\partial}{\partial z}\left(k_z\frac{\partial T}{\partial z}\right)\right] + \dot{Q} \end{aligned} \quad (2.18)$$

2.5 Lumped parameter method

The lumped parameter model (also called lumped element model, or lumped capacitance model) simplifies the description of the behavior of spatially distributed

physical systems into a topology consisting of discrete entities that approximate the behavior of the distributed system under certain assumptions [8].

According to the lumped parameter method, the heat convection is dominant compared with heat conduction, which means that heat conduction is negligible. So, the cell has a uniform temperature. The prerequisite for adopting the lumped parameter method is that the heat convection resistance is much larger than the heat conduction resistance. In some other words, the lumped parameter method proves to be quite precise when $Bi \ll 1$ as described in [8]

$$Bi = \frac{Lh}{k} \tag{2.19}$$

where L is the characteristic length of the solid substance, k is the conductivity of the solid substance and h is the convection coefficient between solid and fluid substance.

To describe the thermal behavior of one cell, the following formula is used

$$\rho V C_p \frac{\partial T}{\partial t} + kA(T - T_\infty) = \dot{Q} \tag{2.20}$$

where ρ is the density of cell, V is the volume of cell, C_p is the specific heat of cell, k is the heat transfer coefficient comprising of both conduction and convection, A is the corresponding heat transfer surface area, T is the cell temperature and T_∞ is the ambient temperature.

The first term of (2.20) is the change of internal energy, the second term shows the heat transfer from cell to ambient and $\dot{Q}$ shows the rate of heat generation.

To solve each transient status of the thermal behavior, the expression can be translated as:

$$T(i+1) = \frac{\dot{Q}\partial t + \partial t A k T_\infty + \rho V C_p T(i)}{\rho V C_p + \partial t A k} \tag{2.21}$$

∂t, which is the temperature calculation interval can defined by the user. When q is constant , the value of ∂t only affects the smoothness of the temperature curve. When $\dot{Q}$ is time-dependant, then the temperature calculation interval ∂t shouldn't be bigger than the updating interval of $\dot{Q}$, otherwise some $\dot{Q}$ signal would be missed.

2.6 Lumped parameter method vs FEA

The reason for employing the lumped parameter method is that while simulating the time-domain rate of heat generation in three dimensions, normally solved by FEA, there will be too much computation in order to solve each transient step, which requires large amounts of simulation time and enough RAM of the computer. Besides, Lee [10] claims that unstructured 3D mesh generation requires great effort to develop a efficient 3D mesh for a given geometry, which requires skills and experience.

It is really low-efficient for such FEA model to do the parameter calibration, especially when modelling the whole battery pack, the temperature gradient in plane is not relatively high, which is found by Ahmed Imtiaz Uddin and Jerry Ku[11].

Compared with the FEA, the lumped parameter method is more simplified because it neglects the temperature gradient of the cell, by considering the cell as a homogeneous object [8]. In other words, the cell temperature is uniform. As a conclusion, such a kind of model is our compromise between accuracy and computation time.

2.7 Single cell equivalent electrical circuits

2.7.1 0 RC circuit model

As shown in Fig. 2.3, this is a simple model and it comprises of an ideal voltage source which is the open circuit voltage U, the cell resistance R_i and the terminal voltage V.

The 0 RC circuit model can be used for fast computations as it requires determining only one parameter which is the cell internal resistance. However, this model fails to capture the electrical dynamic behavior and the same has been highlighted later in section 5.3.1. It is worth mentioning here, that in section 5.1.4, R_{10} resistance has been captured, which is the resistance obtained for a 10 s duration from the pulse tests which is further described in section 4.2.3.

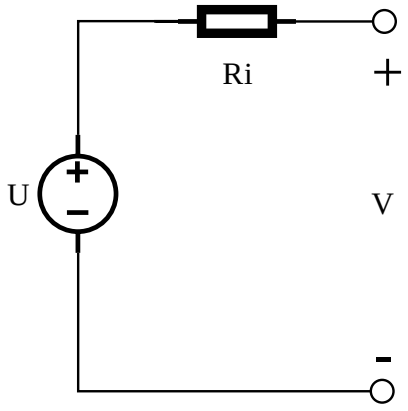


Figure 2.3: 0 RC circuit single cell model

2.7.2 2 RC circuit model

In the 2 RC circuit model, the R_1-C_1 circuit has a faster time constant and the R_2-C_2 circuit has a slower time constant and the reader is directed to Fig. 5.9 in section 5.1.4.

In Fig. 2.4, R_0 represents the bulk resistance of the cell which includes resistances of the electrolyte, separator and the electrodes [38]. R_1 and C_1, R_2 and C_2 are the diffusional dynamics of the cell's impedance [39].

An advantage with the 2 RC circuit model is that it captures the electrical dynamic behavior, but one needs to conduct experiments to determine all the cell parameters such as R_1, C_1, R_2, C_2 which can be time consuming.

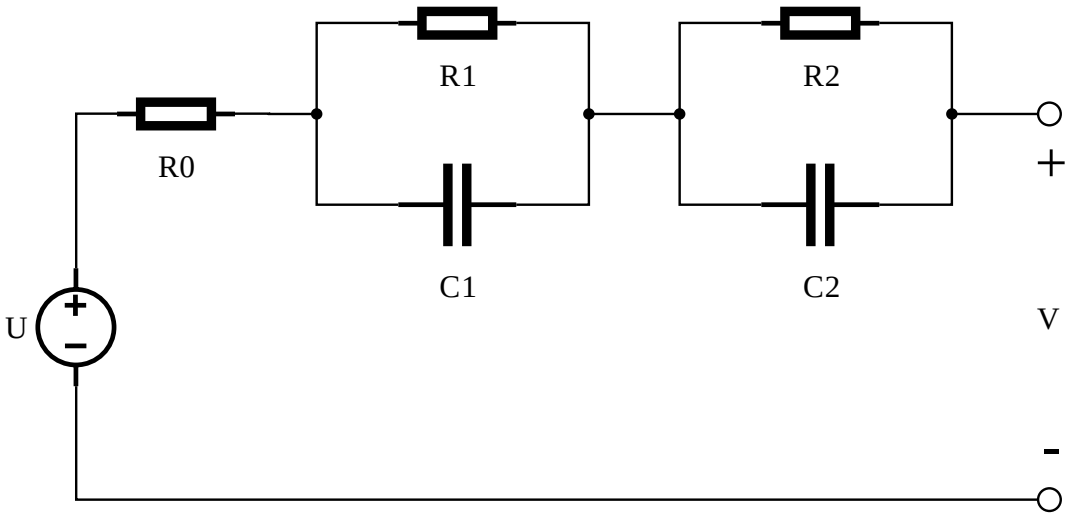


Figure 2.4: 2 RC circuit single cell model

All the resistances R_0, R_1 and R_2 contribute to the joule heat. Bernardi [13], Newman [14] and Thomas Alyea [15] have developed theories explaining the energy balance in an electrochemical system. In a heat transfer analysis, the battery electrochemistry might be modelled with the overall reaction rather than two half reactions in the positive and negative electrodes as expressed in [16]

$$\dot{Q} = I(U - V) + I(T\frac{\partial U}{\partial T}) \tag{2.22}$$

where $\dot{Q}$ represents the total heat generation rate, I is the charge/discharge current (positive under charging and negative under discharging), U is the open circuit voltage, V is the terminal voltage and $\frac{\partial U}{\partial T}$ is the entropic heat coefficient which can be either positive or negative.
Equation (2.22) can be modified to

$$\dot{Q} = I^2 R_i + I(T\frac{\partial U}{\partial T}) \tag{2.23}$$

where the first term on the right hand side of (2.23) represents the irreversible joule heat and the second term denotes the reversible entropic heat as expressed in (2.6) described in section 2.3.4.

3
Case Setup

This chapter is dedicated to the description of the battery pack, the lithium ion cell and a description about the electro-thermal model plan.

3.1 Description of the cell and the battery pack

Table 3.1 shows the single cell characteristics.

Table 3.1: The cell characteristics obtained from the manufacturer's datasheet

Chemistry	Cathode	NCM/LMO (NCM»LMO)
	Anode	Graphite + Amorphous Carbon Blending
	Electrolyte	LiPF6 + EC/EMC based
	Separator	Ceramic coated separator
Design	Packing	Laminated Pouch
	Structure	Stacked
Cell Features	Size (mm)	8.7 (T) x 141 (W) x 162 (H)
	Nominal capacity (Ah)	10 Ah
	Nominal voltage (V)	3.7 V
	Operating voltage (V)	2.5 V - 4.3 V
	Average weight (kg)	0.350 kg
	Specific energy (Wh/kg)	106 Wh/kg
	Volumetric energy (Wh/l)	190 Wh/l

From Table 3.1, NMC»LMO means that the cells are not pure NMC but a blended variety with a much greater percentage of NMC than LMO and the reader is directed back to section 2.3.1 to have a brief understanding of the advantages of different lithium-ion cathode chemistry.

According to the manufacturer

- The cells are power optimized, which means that the battery pack has been designed for hybrid vehicle applications involving high power.
- The maximum battery current is limited to 275 A, due to the electromechanical components such as contactor and fuse.
- The storage temperature of the battery pack is between -40 $°C$ and up to 60 $°C$.
- The cell operating temperature is limited in a range of -30 $°C$ up to 65 $°C$.

Fig. 3.1 and Fig. 3.2 captures the side and front profiles of a part of the dismantled battery pack.



Figure 3.1: A side view photo depicting a part of the dismantled battery pack. One can observe the aluminium plate fitted with air ducts.

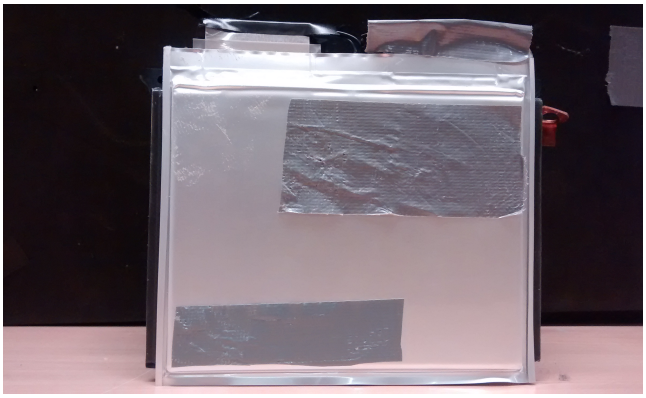


Figure 3.2: A front view photo depicting a cell as a part of the module

As shown in Fig. 3.3 there are 13 cells connected in series electrically and all the cells are stacked like a pack of books on a shelf. There is an aluminium plate between two cells in some modules and very thin air gap between cell and cell in some modules.

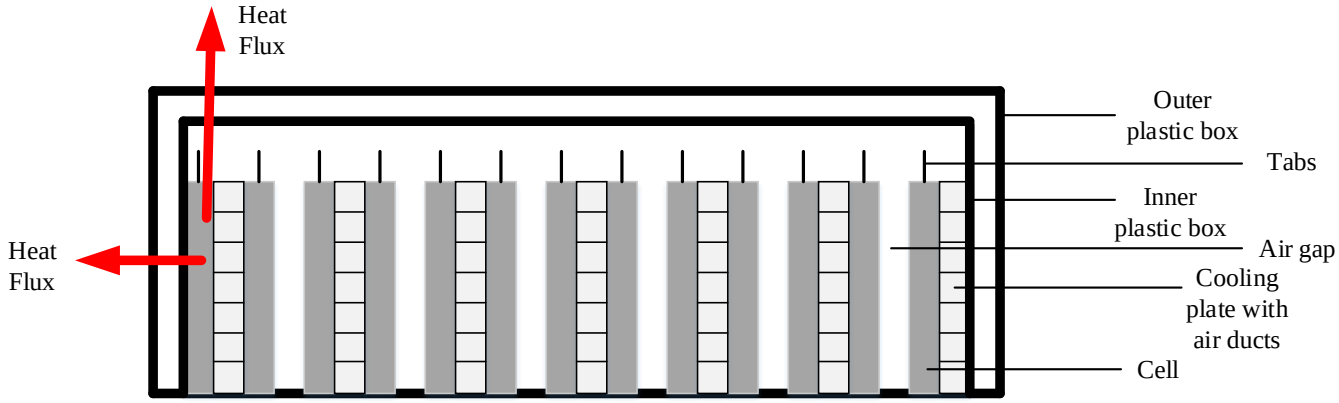


Figure 3.3: An illustration of the 13 cell battery pack as seen from a side. Figure not drawn to scale and electrical connections on the tabs have not been shown to reduce figure complexity.

3.2 General description of the Electro-Thermal Battery Model

Fig. 3.4 presents the electro-thermal battery pack model plan. One can observe that the inputs to the electrical model are the current profiles from the vehicle model block and the initial cell SOC. The electrical model provides the dissipated power(rate of heat generation) to the thermal model, which feeds the temperature back into the electrical model, because the cell temperature affects the electric properties of cell such as the internal resistance and the entropic heat coefficient. The modeling steps have been listed below

1. One cell modeling in one dimension with time-independent rate of heat generation determined using a MATLAB® model based on the Lumped Parameter Method, which is the theory basis for the modelling simplification.
2. One-cell modeling in one dimension with time-independent rate of heat generation using GT-SUITE® based on the lumped parameter method to analyze the thermal behavior of the battery pack.
3. Multi-cell modeling in one dimension with time-dependent rate of heat generation using GT-SUITE® based on the lumped parameter method to analyze the thermal behavior of the battery pack.

For the model verification, temperature measurements at several points of the battery pack have been done and the experimental results have been compared with the simulation results to fine-tune the model.

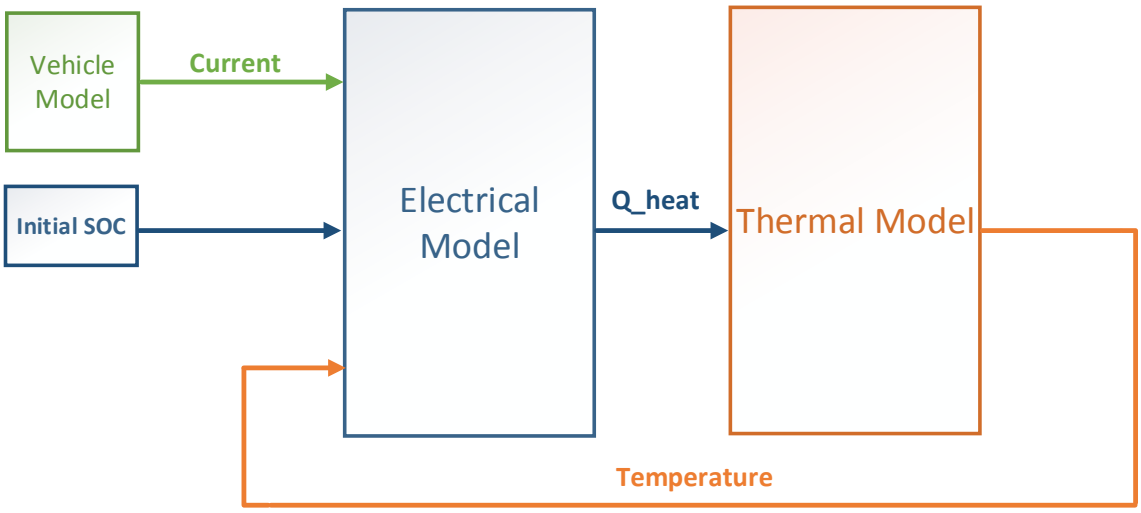


Figure 3.4: The Electro-Thermal Model

3.3 Convection coefficient determination

In this thesis work, both free and forced convection will be discussed because in the model, there is free convection inside the package between the cells and the air and forced convection outside the battery pack because the vehicle climate system and evacuation pressures force the air out from the vehicle as explained by [27].

3.3.1 Free Convection

For free convection in a large volume, the heat convection coefficient (h) is determined using (2.3).

The Nusselt number can be calculated from the Prandtl and Grashof numbers according to [28]

$$Nu = 0.54(Pr \cdot Gr)^{1/4};\ 1.42 * 10^4 < Gr < 1.42 * 10^7 \tag{3.1}$$

$$Nu = 0.15(Pr \cdot Gr)^{1/2};\ 1.42 * 10^7 < Gr < 1.42 * 10^{11} \tag{3.2}$$

Using (3.1) and (3.2) the free convection coefficient in a large space can be calculated as

$$h = \frac{Nu\ k}{L} \tag{3.3}$$

where k is the conductivity of air and L is the characteristic length of the cell.

For the free convection in a confined volume, when the $Gr \leq 2430$, conductive heat transfer will be dominant between the two substances; for $Gr \geq 2430$, convective heat transfer between the two substances will assume significance [28]. For such cases, the Nusselt number can be obtained, using the following expressions as specified in [28]

$$Nu = 0.212(Pr \cdot Gr)^{1/4};\ 1.0 * 10^4 < Gr < 4.6 * 10^5 \tag{3.4}$$

$$Nu = 0.061(Pr \cdot Gr)^{1/3};\ Gr > 4.6 * 10^5 \tag{3.5}$$

Using (3.4) the heat convection coefficient (h) in a limited space can be calculated as considered in (3.3).

3.3.2 Forced Convection

Reynolds number (Re) is the decisive factor for the heat convection coefficient in forced convection and it depends upon the air flow velocity.

Nusselt number (Nu) is related to the Reynolds and Prandtl (Pr) numbers as expressed in [28]

$$Nu = 0.664 \cdot Re^{1/2} \cdot Pr^{1/2} \tag{3.6}$$

By substituting (2.4) and (3.6) into (3.3) the heat convection coefficient (h) for forced convection can be calculated.

3.4 Contact conductance

In our case, there is perfect contact conductance between the cell and the aluminium plate, which was observed once we dismantled the battery pack.

M.M.Yovanovich [29] did research on the calculation of thermal joint resistance for the interface formed by two conforming, rough surfaces. Antonetti and Yovanovich [30] further used and described the model of thermal joint conductance (h_j) which is formed as

$$h_j = h_c + h_g \tag{3.7}$$

where h_c is the contact conductance and h_g is the gap conductance.

M.G.Cooper [31] approximated the equation describing contact conductance in 1968 as

$$h_c = 1.45 k_s \frac{m_s}{\sigma_s} \left(\frac{P}{H_c} \right)^{0.985} \tag{3.8}$$

and M.M.Yovanovich [29] further modified (3.8) to

$$h_c = 1.25 k_s \frac{m_s}{\sigma_s} \left(\frac{P}{H_c} \right)^{0.95} \tag{3.9}$$

where P is the contact pressure, H_c is microhardness of the softer of the two contacting materials, k_s is the harmonic mean thermal conductivity of the interface [29], which can be calculated as

$$k_s = \frac{2k_1k_2}{k_1 + k_2} \tag{3.10}$$

where k_1 and k_2 are the thermal conductivities of the two materials, σ_s is the RMS value of surface roughness [29], which is formulated as:

$$\sigma_s = \sqrt[2]{\sigma_1^2 + \sigma_2^2} \tag{3.11}$$

where, m_s is the RMS value of the asperity slope [29], which is expressed as:

$$m_s = \sqrt[2]{m_1^2 + m_2^2} \tag{3.12}$$

VW Antonetti [32] also approximated the relation between m_s and σ_s due to the difficulty in finding the asperity slope value, as:

$$m = 0.125(\sigma * 10^6)^{0.402};\ 0.216\mu m \leq \sigma \leq 9.6\mu m \tag{3.13}$$

As for the gap conductance, h_g, Yovanovich [33] approximated the expression as:

$$h_g = k_g/(Y + M) \tag{3.14}$$

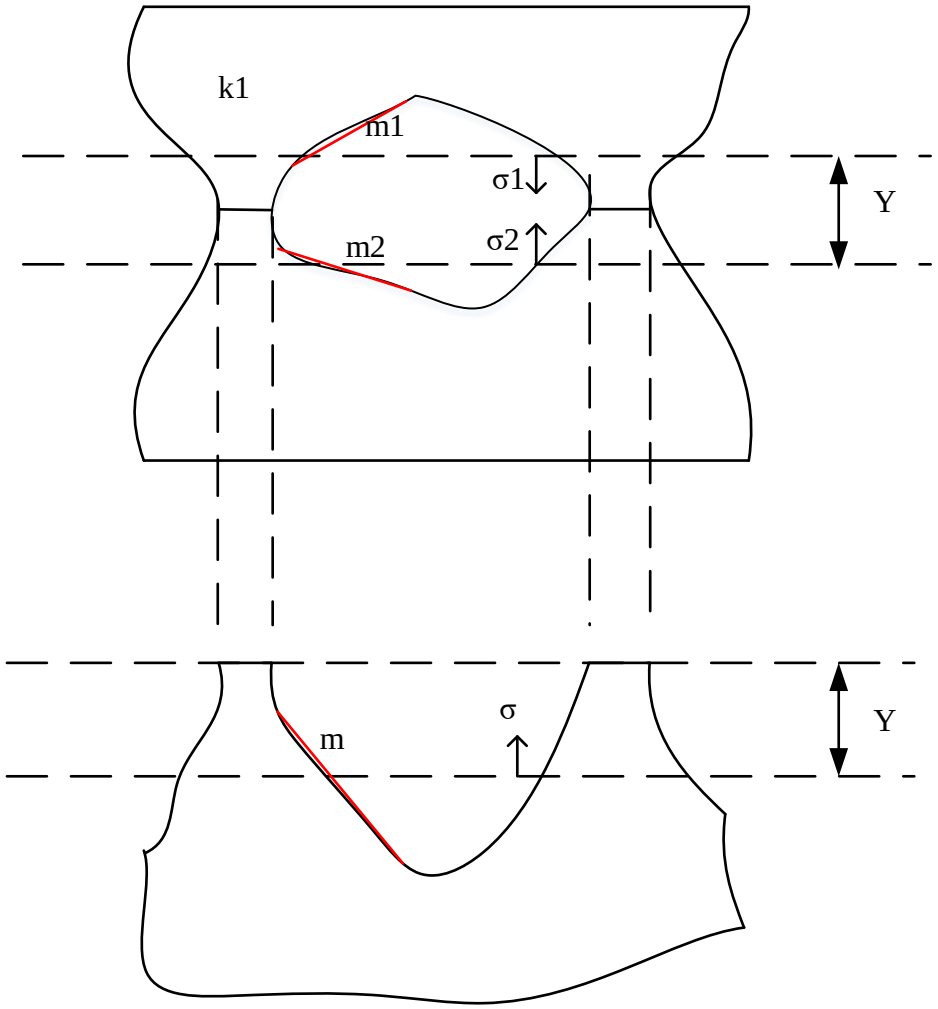


Figure 3.5: An illustration of conforming rough surfaces adapted from [29].

where k_g is the thermal conductivity of the gap substance and Y as the effective gap thickness shown in Fig. 3.5 [33] ,which can be precisely calculated through the expression with the simple power-law correlation equation proposed by Antonetti and Yovanovic [30]:

$$Y = 1.53\sigma(P/H_c)^{-0.097}; 10^{-5} \leq P/H_c \leq 2 * 10^{-2} \tag{3.15}$$

The gas parameter M takes into account the rarefaction effects at high temperatures and low gas pressure, and this parameter depends on the thermal accommodation coefficients, the ratio of specific heat, Prandtl and molecular mean free path of the gas[29]. The expression showing the relationship between gas parameter M and the

gas pressure, temperature is expressed as in [29]:

$$M = M_0 \frac{T}{T_0} \frac{P_0}{P} \tag{3.16}$$

where M_0 means the gas parameter value at the reference values of gas temperature and pressure T_0, P_0 respectively. And reference values of the gas parameter for air is shown in table 3.2

Table 3.2: Material properties of the gap substance

Gap substance	Thermal conductivity $W/(m \cdot K)$	Gas parameter $M_0 * 10^6$,m
Air	0.026	0.373 [29]
Thermal grease	0.2-0.7 [29]	0.0
Doped thermal grease	1.68-2.58 [29]	0.0

$T_0 = 50° \ C$; $P_0 = 1 \ atm$

Table 3.3: Material properties

Material	Thermal conductivity $W/(m \cdot K)$	Microhardness MPa	Surface roughness μm
Cell	0.8 (in depth) 30(in plane)	/	/
Aluminium	201 [29]	1094 [29]	0.4 (flycut) [29]
Polypropylene	0.11-0.17	107.877	0.8 [34]

At this point, we would like to encourage the reader to go through section 5.2 to connect the theory described above with the results.

3.5 Single cell electro-thermal model using GT-SUITE®

3.5.1 Single cell electrical model

From Fig. 3.6, it can be seen that the single cell electrical model comprises of calculation blocks which includes the SOC calculation block, the internal resistance look-up (resistance as a function of both SOC and temperature), the open circuit voltage look-up and the entropic heat coefficient look-up for the entropic heat function block.

The purpose of the SOC block is to estimate the SOC of the cell based on the initial SOC status and then integrate the product of current and corresponding time interval. The lookups for the internal resistance, the open circuit voltage and the entropic heat coefficient look-up are meant to update the cell electrical parameters in real time, depending on the inputs temperature and the SOC condition.

We have adopted two RC circuits to simulate the dynamic behavior for the single cell electric aspect. The reason is that the time constant for the first RC block is in the magnitude of 10 s and for the second RC block, it is in the magnitude of 100 s, which can represent our constant current at 2C (20 A) loading case well.

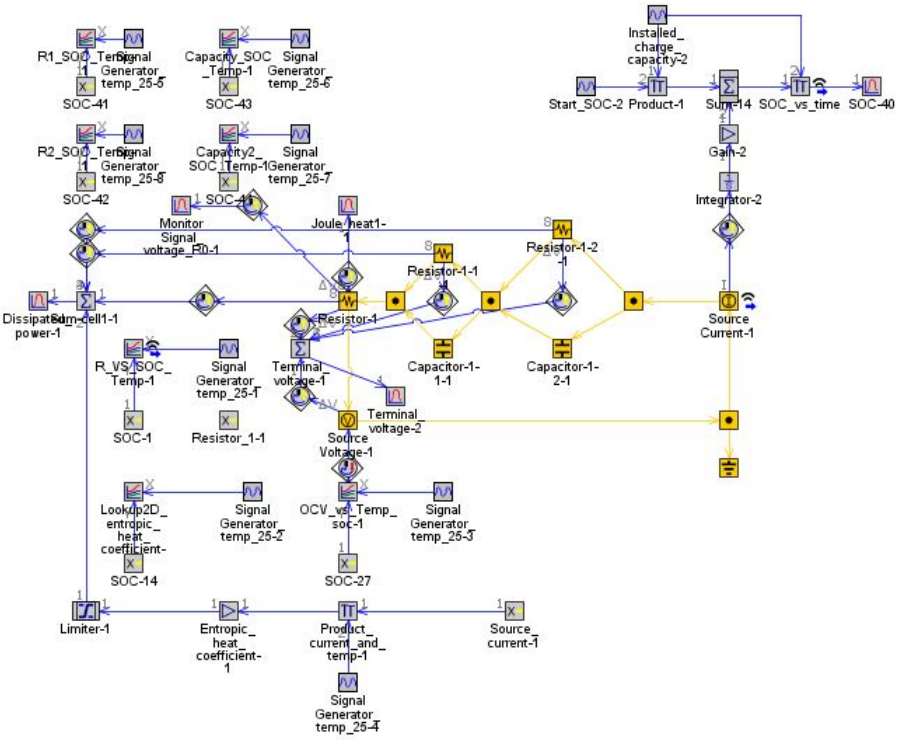


Figure 3.6: Single cell 2 RC circuits simulation model

3.5.2 Single cell thermal model

Fig. 3.7 shows the single cell thermal model. Six thermal masses represent the polypropylene (plastic) package surrounding the cell stack and the 'Piperectangle-1' block is adopted to represent the air volume inside the battery pack. The 'External-cooling-air' block symbolizes the cooling air outside the package. The difference between both of them is that the 'Piperectangle-1' is blocked from both ends while the 'External-cooling-air' has an inlet flow. The reason for this is that, during the lab measurements the same battery pack was sealed off with insulation tape to prevent any cooling air into or out of the package.

As discussed in section 3.3.1, the cooling condition of the air inside the battery pack fits the free convection in a confined volume, so (3.4) is adopted for the Nusselt number calculation.

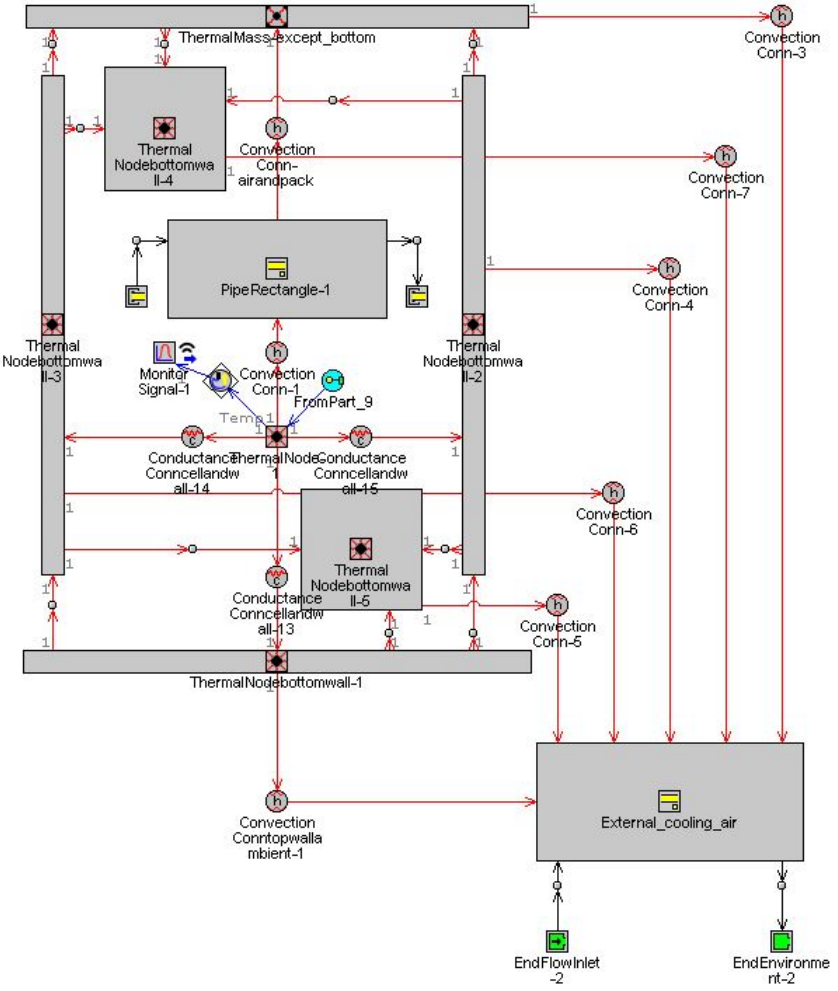


Figure 3.7: Single cell thermal simulation model

Fig. 3.8 depicts the convection coefficient between the air and the cells. Initially, there is only thermal conductivity and as the temperature difference between the air and the cells increase, the air flow becomes more faster, after the Grashof number reaches 2430 in accordance with [28] , the heat transfer turns to be convection.

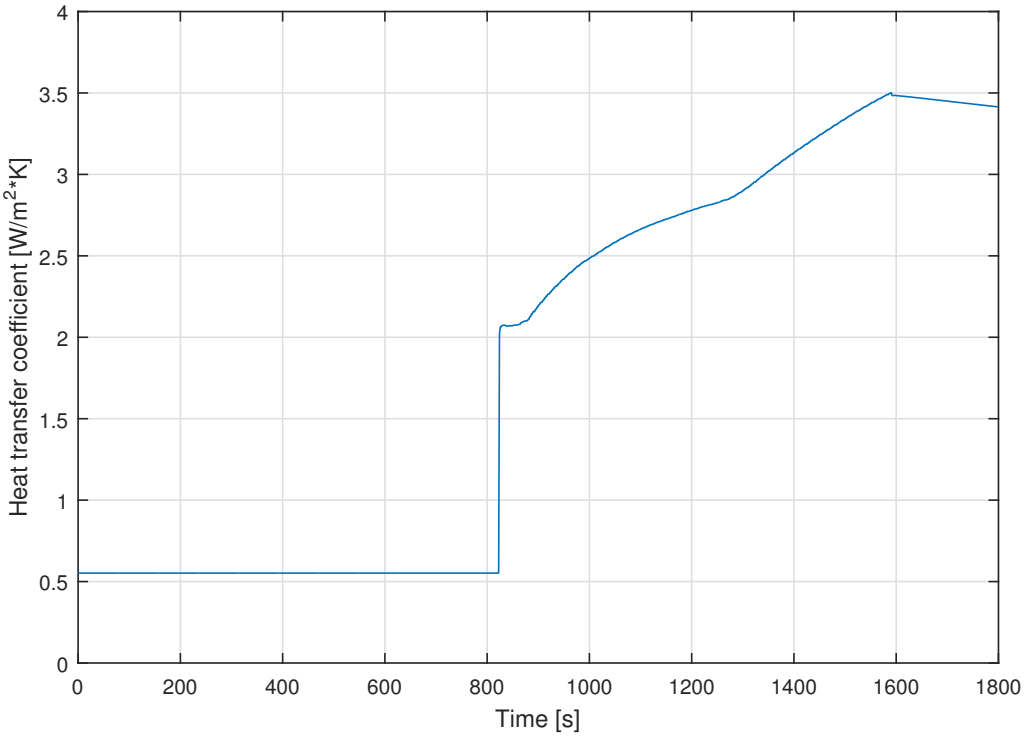


Figure 3.8: Simulated heat transfer coefficient inside the battery pack

4

Experiment

In this chapter we have described the experimental procedures employed to test the battery pack, one single cell with an aluminium cooling plate and a module comprising of two cells with an Aluminium plate in between them.

4.1 48 V battery pack experiments

4.1.1 Application of a constant current to the battery pack

4.1.1.1 Purpose

The main aim is to observe the cell temperature behavior inside the pack. The experiment is carried out for two different temperatures of 10 and 35 $°C$.

The motivation for choosing these two values is due to the fact that we want to study the thermal behavior of the battery pack at a low temperature and at a higher temperature, but at the same time we do not want to expose the battery to extreme temperature cases (for example temperatures greater than 60 $°C$ and less than 0 $°C$.) because we are of the opinion that there should be a battery management system installed on the pack which would monitor the pack temperature and keep the battery pack within its safe operating temperature range [35].

4.1.1.2 Procedure

The first stage involves prepping up the battery pack with the temperature sensors at the locations which are of interest to us for studying the thermal behavior.
Fig. 4.1 shows the battery pack inside the climate chamber.



Figure 4.1: The battery pack inside the climate chamber fitted with temperature sensors both inside and outside the battery pack.

The gray color insulation tape on the side of the pack is used to seal off an air flow vent. All other air pockets on the battery pack are also sealed using the insulation tape. The temperature measurements are recorded on a Fluke Hydra data acquisition unit.

In the next stage we discharge the battery pack with a constant current (2C in our case) using an electronic load in the battery mode as shown in Fig. 4.4.

4.1.2 Application of a charge-discharge current to the battery pack

4.1.2.1 Purpose

The main goal of this experiment is to analyze the temperature behavior of the battery pack under a charge-discharge pulsed current. This is adopted to simulate real driving cycle conditions and the experiment is carried out for a temperature of 25 $^{\circ}C$.

The Digatron equipment needed to charge/discharge the battery with a programmable test setup was unavailable during the relevant time period. As a way around, we have used a 300 V power supply to charge the pack and an electronic load set to battery mode to discharge the pack.

4.1.2.2 Procedure

An electronic load and a power supply are employed to discharge and charge respectively with 2C current for 360 s. The SOC range is decided to be between 39 % and

59 %, because this is the optimal SOC range for a mild-hybrid application [40].

Initially, the battery pack is discharged to 39 % SOC with a 2C rate current and the battery pack is rested for an hour to allow the chemical reactions inside the battery pack achieve an equilibrium condition (relaxation phase). This is the starting point for the experiment.

Next, the power supply is used to charge the battery pack with a 2C rate current for 360 s thereby, increasing the SOC from 39 % SOC to 59 % SOC. Subsequently, the electronic load is employed to discharge the battery pack from 59 % SOC to 39 % SOC and two more charging and discharging pulses are conducted. Fig. 4.2 portrays the charge -discharge pulses applied to the battery pack.

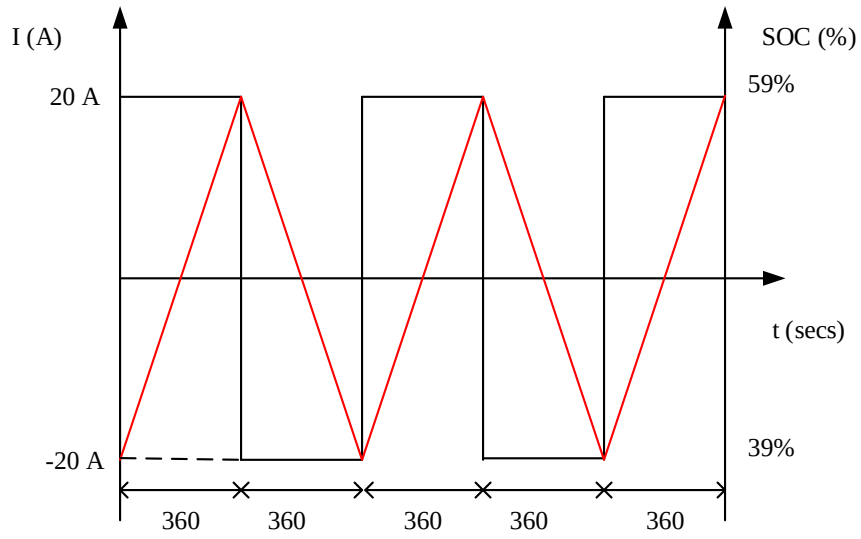


Figure 4.2: An illustration of the charge discharge current pulse, where each pulse was applied for 360 seconds. The sawtooth SOC had been maintained between 39 % and 59 % SOC.

Fig. 4.3 represents the 300 V power supply used for the experiment.

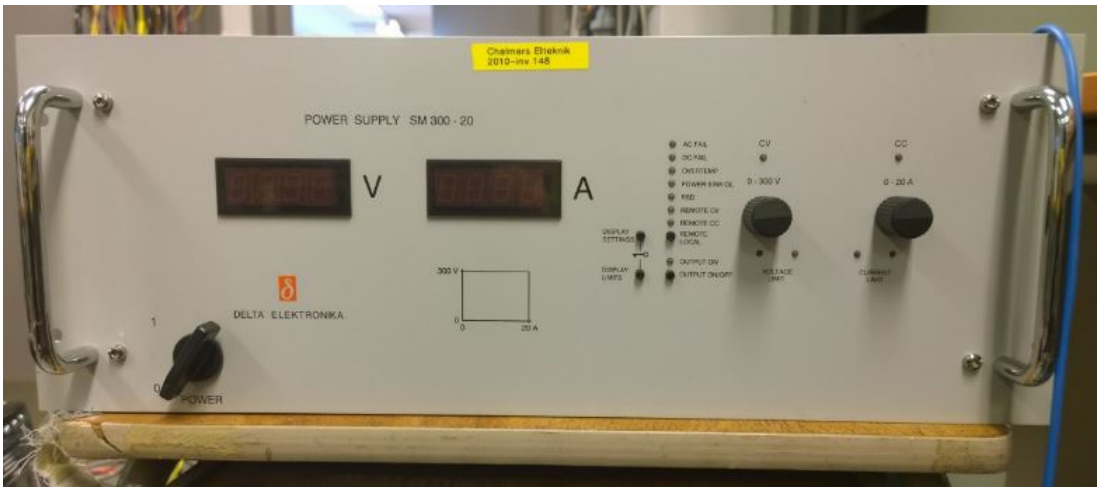


Figure 4.3: A photo of the 300 V power supply used to charge the battery pack. The model used is SM300-20 from Delta Elektronika.

Fig. 4.4 depicts the electronic load used for the experiment.

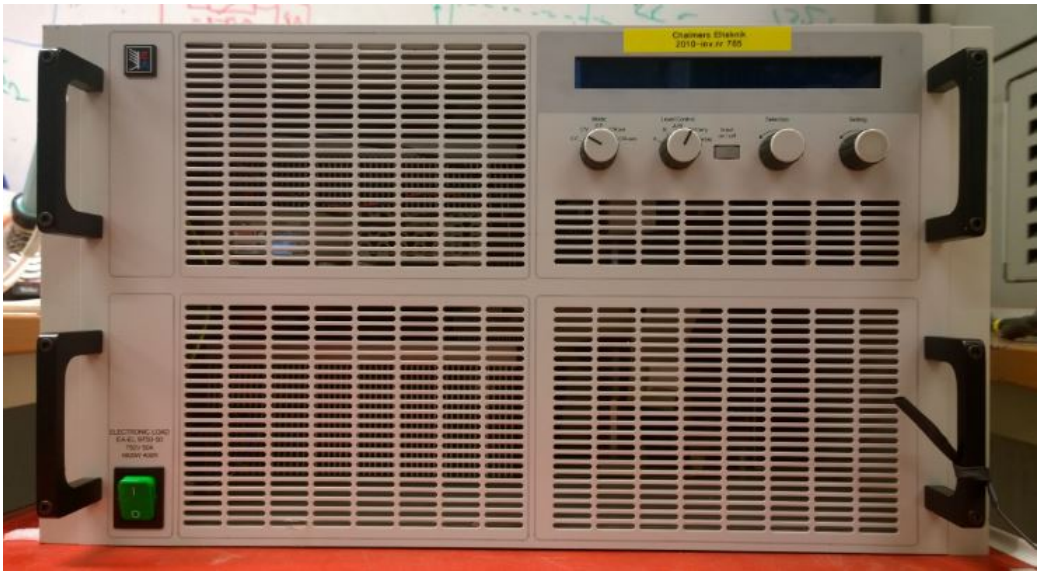


Figure 4.4: A photo of the electronic load used to discharge the battery pack. The model used is EA-EL 9750-50 and it has a rating of 750 V, 50 A and 4800 W.

4.1.3 Test Conditions

1. The temperature of the climate chamber is set to one specific temperature to simulate the ambient temperature.
2. When the battery pack loading started, the climate chamber is switched off, because no extra heat source is needed during the test.
3. The thermo couples are used in the following locations:
   (a) the air temperature of the internal air (air inside the battery pack).
   (b) the air temperature of the external air (air outside the battery pack).
   (c) the temperature of the battery pack (top,right,left and bottom).

(d) the temperature of the cell surface.

4. The battery pack is originally designed for forced cooling and it is supplied with a cooling fan, which has later been removed and the air vents inside the battery pack is sealed. This is done in accordance with a discussion with [40].
5. All the cell voltages are checked with a multimeter to ensure they are all balanced, before being loaded.
6. The power supply and the electronic load have to be programmed for the upper and lower voltage limits, which are 55.25 V and 37.05 V respectively.

4.2 Experiments on a single cell attached to an aluminium cooling plate

4.2.1 Purpose

The following experiments are conducted to extract the single cell parameters which have to be set as inputs for the look up tables inside the simulation model such as the look up table of $\frac{\partial U}{\partial T}$ (entropic heat coefficient) and the cell parameters such as R_0, R_1, R_2, C_1, C_2 and C_p (specific heat).

4.2.2 Experiment 1: Nominal capacity and open circuit voltage measurement

4.2.2.1 Purpose

In order to estimate the real time SOC status of the lithium-ion cell with the known initial SOC status and the current profile, it is necessary to extract the capacity data.

Another way to estimate the SOC status of the cell is by referring to the open circuit voltage as shown in Fig. 4.5. In addition, with the open circuit voltage curves, the entropic heat coefficient, $\frac{\partial U}{\partial T}$, can be approximated as well.

4.2.2.2 Procedure

1. The cell is placed inside the climate chamber and is charged to 100 % SOC during thermal equalization.
   (a) The climate chamber is set to the anticipated temperature.
   (b) The cell is charged with a constant current at 0.1C rate (1 A) until the upper voltage limit is reached (4.25 V).
   (c) There is an electrical relaxation period for 60 minutes after charging and we make sure that the cell reached the anticipated temperature by checking the temperature measured using the thermo couples attached to the cell. We make sure that the cell reached its thermal equilibrium (steady state temperature).
2. The cell is discharged to 0 % SOC and the voltage, current and temperature readings are logged simultaneously every 6 seconds.

(a) The cell is discharged with a constant-current of 0.1C rate (1 A) until it reached the lower voltage limit (2.8 V).

3. The cell is rested for 60 minutes (electrical relaxation)

4. The cell is charged to 100 % SOC and the voltage, current and temperature readings are logged simultaneously every 6 seconds.

   (a) The cell is charged with a constant-current at 0.1C rate (1 A) until the upper voltage limit is reached (4.25 V).

5. The above procedure is repeated for different temperatures.

The open circuit voltage is obtained as the mean value of the open circuit voltage measured during charging and the discharging phases as shown in Fig. 4.5. Also, the cell capacity is calculated by accumulating the product of current and time during the charging and discharging phases respectively and then the mean value is obtained.

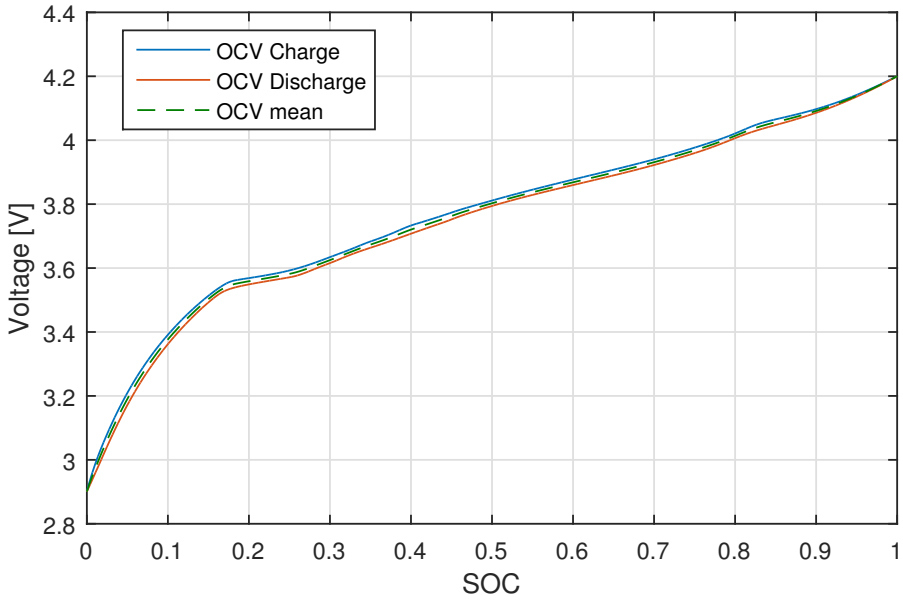


Figure 4.5: Measured data of the mean value of the open circuit voltage for a single cell obtained at 0.1 C-rate charge/discharge current for different SOC points. The experiment was performed for temperatures of

Fig. 4.6 shows the potentiostat which is programmed to load the cell and it has a current limit of 3 A. The advantage of using the Gamry potentiostat is that it can achieve a high resolution for the voltage measurement whose resolution is of the order of 10^{-5} V.



Figure 4.6: A photo of the potentiostat. Model used is Reference 3000 from Gamry Instruments.

4.2.3 Experiment 2: Cell impedance measurements

4.2.3.1 Purpose

The purpose of this experiment is to measure the battery cell impedances with 2C rate (20 A) current at different temperatures for the SOC window from 0 % to 100 %.

4.2.3.2 Procedure

1. As the initial cell charge state (Ah) is unknown, the cell is charged to 100 % SOC at 2C rate (20 A) and rests for 60 minutes.
2. The cell is discharged with a current of 2C rate (20 A) for a 150 s pulse and after each discharge pulse, the cell is rested for 60 minutes.
3. Totally, 12 discharge pulses are needed to discharge the cell from 100 % SOC to 0 % SOC.
4. The aforementioned steps are repeated for different anticipated temperatures.
5. The reason for having the relaxation phase is because the R_1, C_1, R_2 and C_2 values have to be obtained for a stable phase SOC rather than at a transition phase i.e the cell has to attain electrical relaxation and the reader is directed to refer Fig. 2.4.

4.2.4 Experiment 3: Determination of the specific heat C_p value

4.2.4.1 Purpose

The heat capacity of the battery pack plays a high role in the thermal behavior, especially for the time constant of the system as shown in (5.1). So, this experiment is designed to measure the specific heat ($\frac{J}{kg \cdot K}$) of the cell.

4.2.4.2 Procedure

1. An insulation box is prepared to house the test cell and the dummy cell. The insulated box is sealed off with an insulation tape. Dummy cell is the copper wire and test cell is the lithium cell together with the aluminium cooling plate. The purpose of the dummy cell is to heat up the test cell and from (4.1), one can observe that by knowing the voltage and the current the dissipated power from the dummy cell can be calculated.

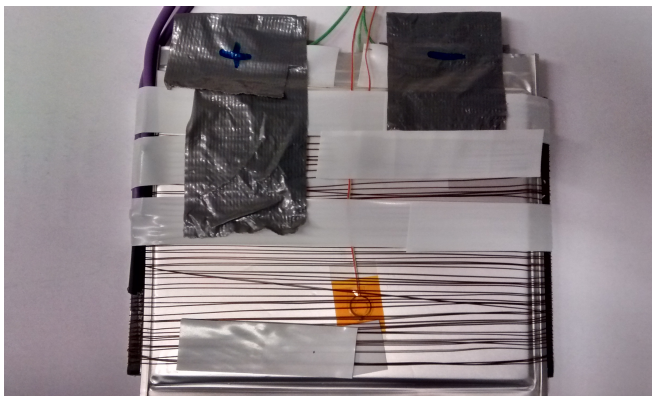


Figure 4.7: A photo of the test cell together with the dummy cell. The orange tape consists of a thermocouple attached to the cell surface for temperature measurement. A total of 6 thermocouples (2 for the tabs, 1 for the aluminium cooling plate and 2 for the cell body temperature measurement) have been used in this experiment

   We would like to clarify that, the test cell comprises of only a single lithium-ion cell with the aluminium plate and a dummy cell which is just the copper wire wrapped around the test cell.
2. The specific heat of the dummy cell $C_{p,dummy}$ ($\frac{J}{kg \cdot K}$) and the aluminium cooling plate $C_{p,al}$ ($\frac{J}{kg \cdot K}$) are referred from [41]. Besides, even with a good insulation box, there is still some leakage which can not be avoided and we define the leakage thermal resistance as R_{th} ($\frac{K}{W}$) and the total heat capacity as C_{th} ($\frac{J}{K}$) which includes the heat capacity of the dummy cell, the test cell, the aluminium plate and the insulated connecting wires as shown in Fig. 4.8.
3. The test cell together with the dummy cell is heated inside the insulation box for a time duration $t(s)$ and during this time duration, the climate chamber is turned off. The total heat capacity is approximated using

$$P - \frac{T_{cell} - T_{ambient}}{R_{th}} = C_{th}\frac{dT_{cell}}{dt} \tag{4.1}$$

where P is the rate of heat generation from the dummy cell and $T_{ambient}$ is the air temperature within the climate chamber.



Figure 4.8: The sealed white insulation box comprising of the test and dummy cell inside the climate chamber.

4.2.5 Risk Analysis

As a preparation towards the experiment plan, we have prepared a risk analysis plan which has been presented below.

1. The lower and upper open circuit voltage limit of the cell can be estimated as 37 V/13 cells = 2.85 $V/cell$ and 54 V/13 cells = 4.15 $V/cell$ respectively. The datasheet from the supplier defines the cell limits as $V_{min} = 2.5V$ and $V_{max} = 4.30V$. The transient limits (terminal voltages) specified by the manufacturer give us greater freedom to extract power over a wider range of SOCs. The steady state voltages (OCV) define the 0 %-100 % SOC range.
2. The Digatron should be programmed to shut down the experiment, if the steady-state voltage exceeds 4.25 V or goes below the lower voltage limit of 2.8 V.
3. According to the supplier datasheet, the optimal battery operating temperature should be 40 °C. For temperatures greater than 45 °C the allowed battery current would be reduced and if the battery temperature exceeds more than 55 °C, the allowed battery current is set to zero.
4. The battery cell operating temperature is limited to the range of -30 to 65 °C. The initial cell temperature is set to be 10 or 30 °C as per the experiment plan to simulate Sweden or Arizona ambient temperature.
5. The datasheet specifies the maximum battery current to be 275 A due to electromechanical components (contactor and fuse).

5

Results

In this chapter, the results generated from both the simulation model and the experiments have been presented for both the battery pack and the battery cell.

5.1 Experiment results

5.1.1 Cell capacity at different temperatures for both charging and discharging

Fig. 5.1 shows that both the charging and discharging capacity of the cell increases with temperature. Also, the cell charging capacity is more sensitive to temperatures than the discharging capacity. For temperatures greater than approximately 303 K the cell has a larger charge capacity and at lower temperatures, the cell has a larger discharge capacity. The reasons for this result could not be explained.

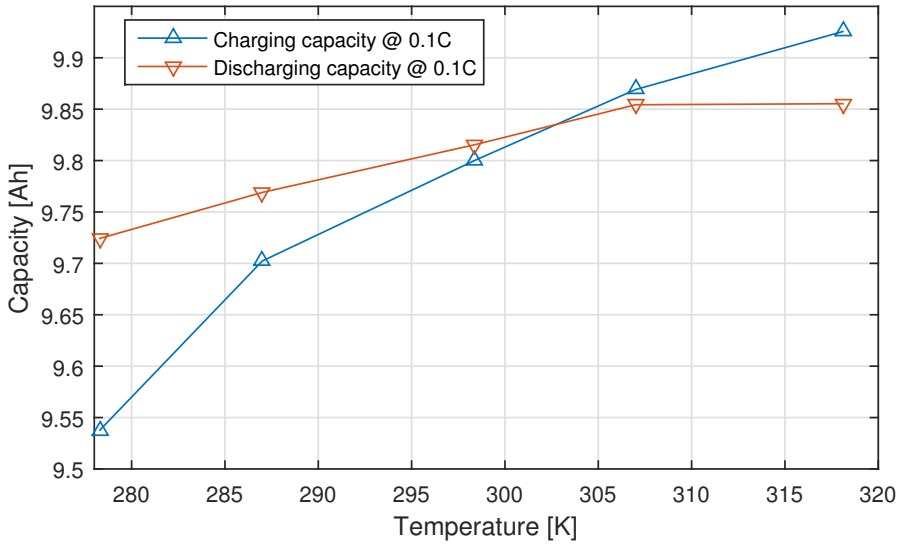


Figure 5.1: Charging and discharging capacity of the cell under different temperatures at 0.1 C rate.

From Fig. 5.2, it can be observed that discharging with different C rates, creates an obvious difference in the discharge capacity of the cell.

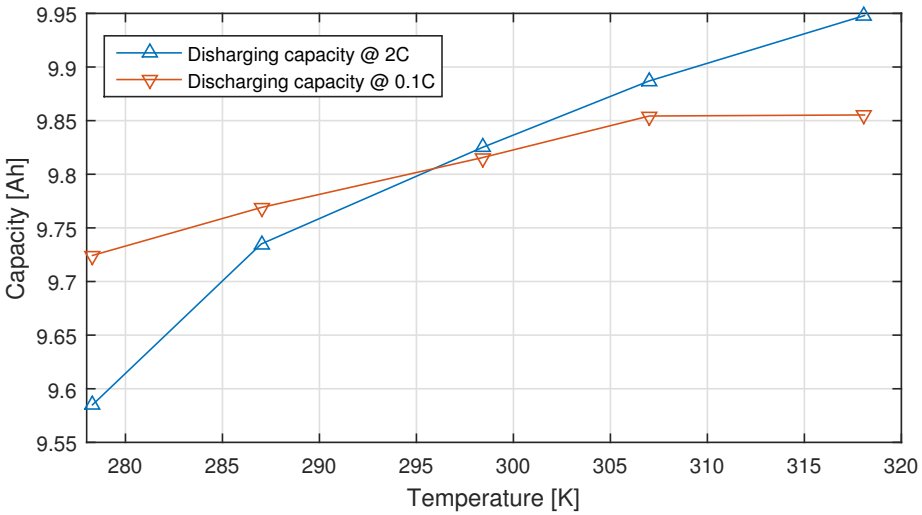


Figure 5.2: Discharge capacity of the cell for different temperatures at 0.1 C and 2 C rate.

5.1.2 Open circuit voltage as a function of SOC and temperature

Fig. 5.3 and Fig. 5.4 shows the raw data of the cell open circuit voltage and the cell open circuit voltage after data reduction and interpolation respectively. We can infer that the open circuit voltage varies with SOC, while the temperature has a minor influence on the open circuit voltage determination.

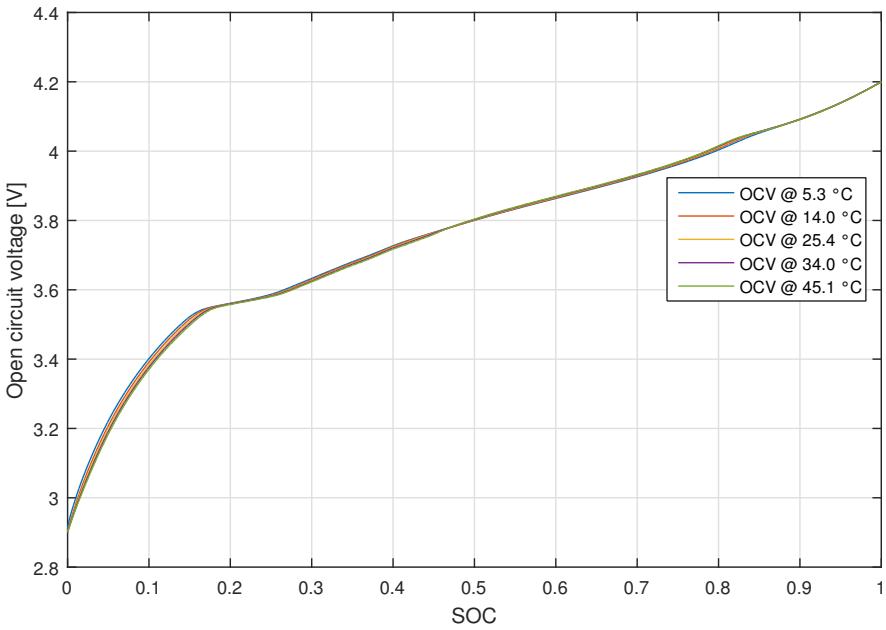


Figure 5.3: Raw data of the cell open circuit voltage as a function of temperature and SOC obtained under 0.1 C-rate charge and discharge current

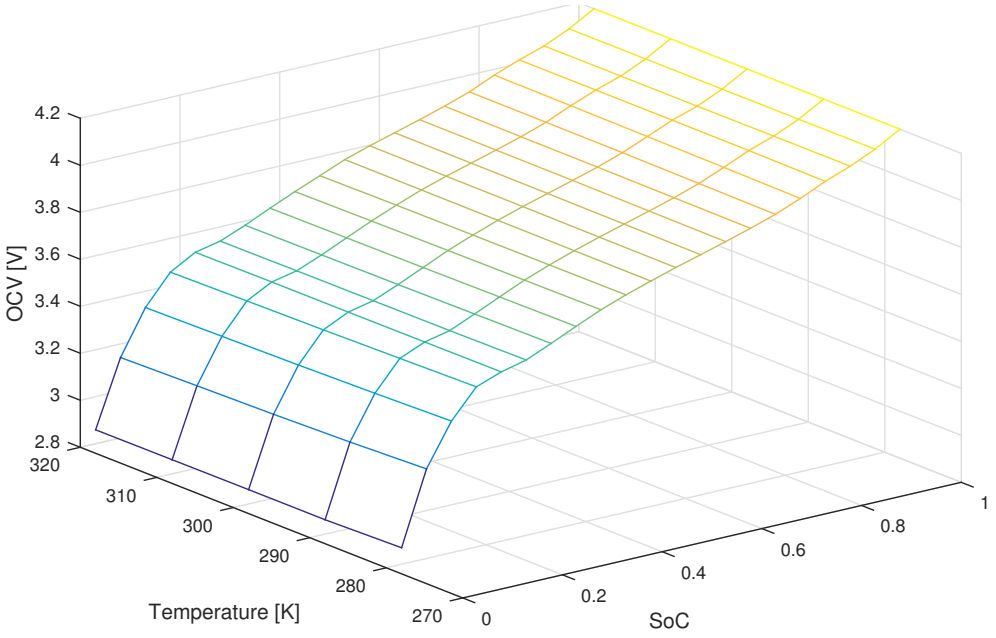


Figure 5.4: Processed data of a single cell open circuit voltage as a function of temperature and SOC

5.1.3 Entropic heat coefficient depending on SOC and temperature

Fig. 5.5 and Fig. 5.6 consist of the raw data of the entropic heat coefficient and the entropic heat coefficient obtained after data reduction and interpolation respectively. The reason for the fluctuation in the entropic heat coefficient at 40 $°C$ is unknown.

From Fig. 5.5 and Fig. 5.6, we can infer that both the temperature and the SOC play a dominant role on the entropic heat coefficient and we can see that as the temperature decreases, the magnitude of the entropic heat coefficient increases. The entropic heat coefficient was obtained by taking the difference between two open circuit voltages divided by the temperature difference.

We can see that the entropic heat coefficient is negative up to approximately 45 % SOC and then it changes the sign, i.e the battery may shift from endothermic to exothermic reaction and in section 5.1.5 we have verified the existence of entropic heat. Some interesting crests have been captured at 20 % and at 80 % SOC.

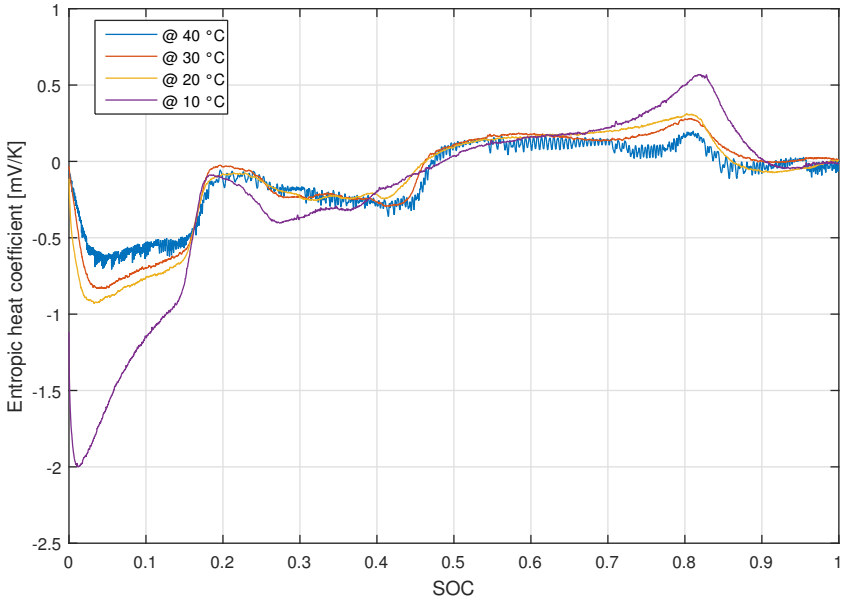


Figure 5.5: Raw data of the entropic heat coefficient depending on temperature and SOC

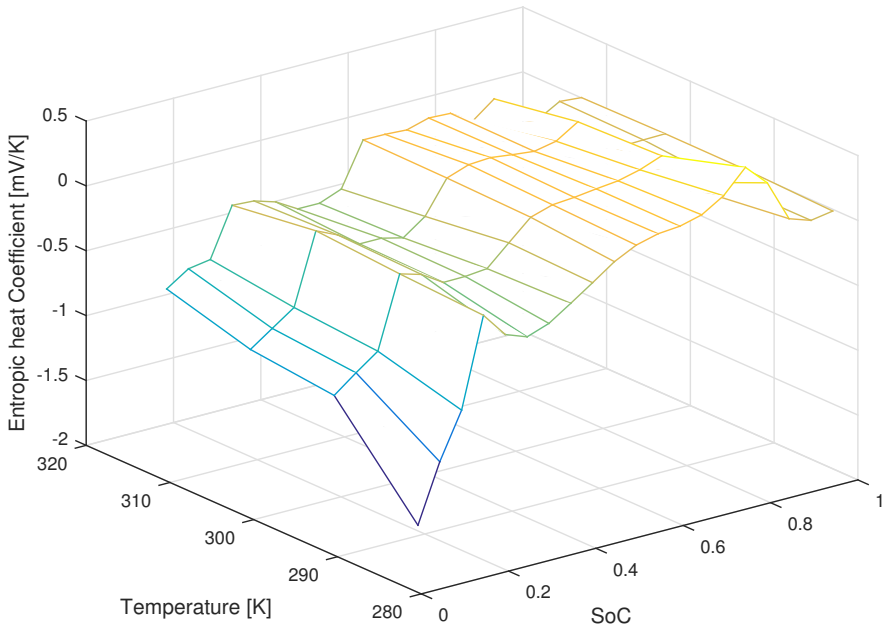


Figure 5.6: Entropic heat coefficient depending on temperature and SOC

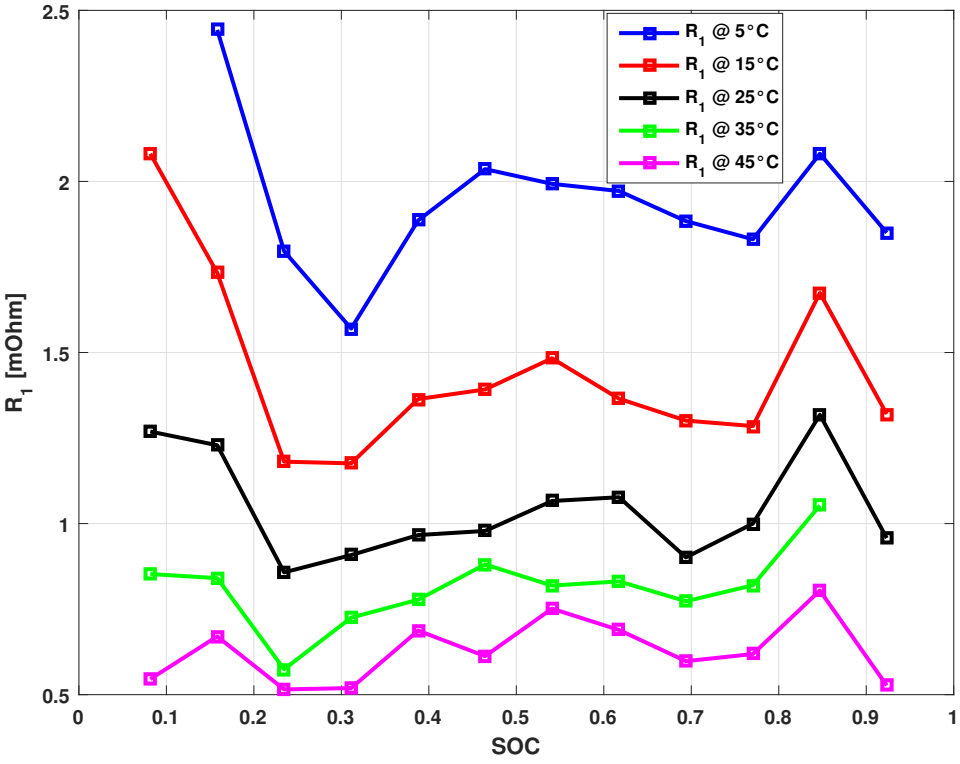
5.1.4 Cell impedance measurements

From Fig. 5.7a, we can infer that the resistance values increase with decreasing temperatures, which can be attributed to the fact that at lower temperatures the lithium-ion batteries have a poor performance due to poor electrolyte conductivity,

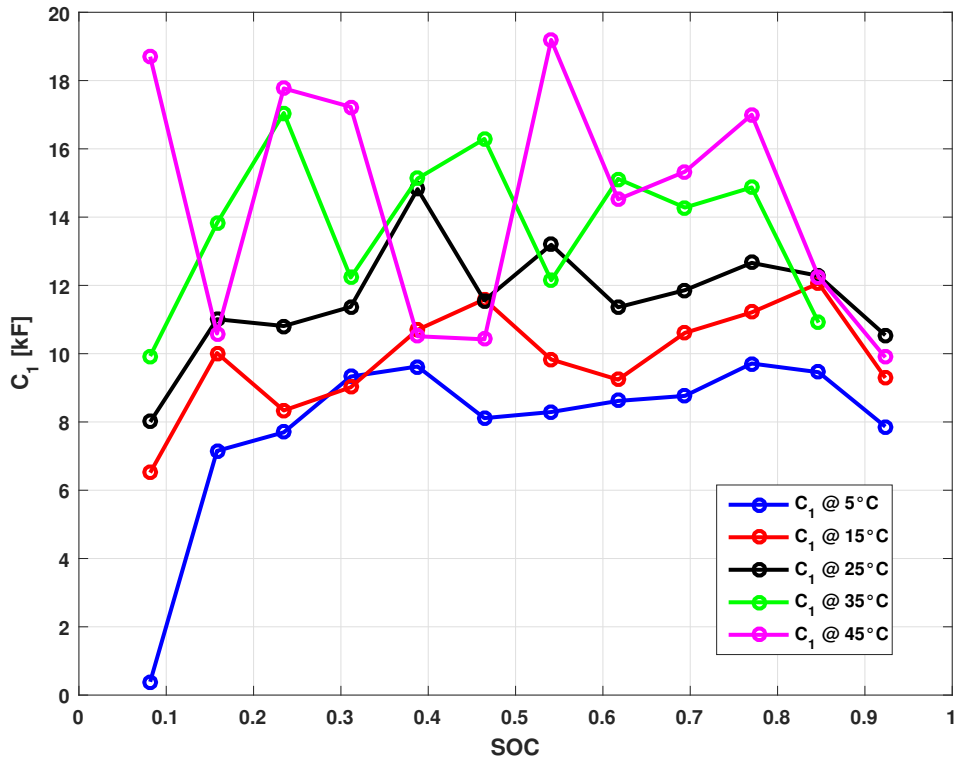
sluggish charge transfer kinetics, increased resistance of solid electrolyte interphase (SEI) and slow Lithium diffusion through the surface layers and through the bulk of active material particles [38]. Conversely, at higher temperatures the resistance values are lower. Thus, there will be lower losses at higher temperatures and vice versa. An interesting phenomenon is observed around 78 % to 91 % SOC for R_1, where the resistance first increases and then decreases for the different temperatures. However, we could not justify the reason for the same.

Fig. 5.7b, shows that the capacitance values increase with increasing temperatures which is in accordance with [37]. We could not analyze the reason for the zigzag behavior of C_1.

Fig. 5.8 shows a similar trend, where we obtain a higher resistance value at lower temperatures and a lower resistance value at higher temperatures. Again, we observe an interesting behavior between 70 % to 90 % SOC. As discussed earlier, the capacitance value increases as the temperature increases, but this time we can observe less zigzag behavior as compared with Fig. 5.7b.

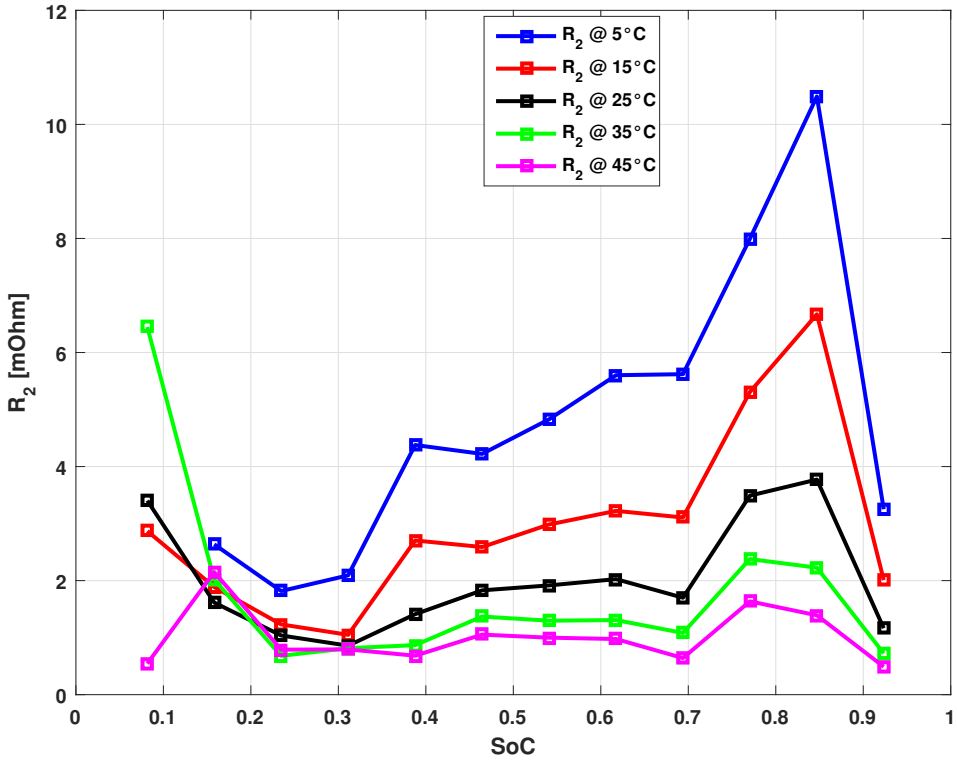


(a) R_1

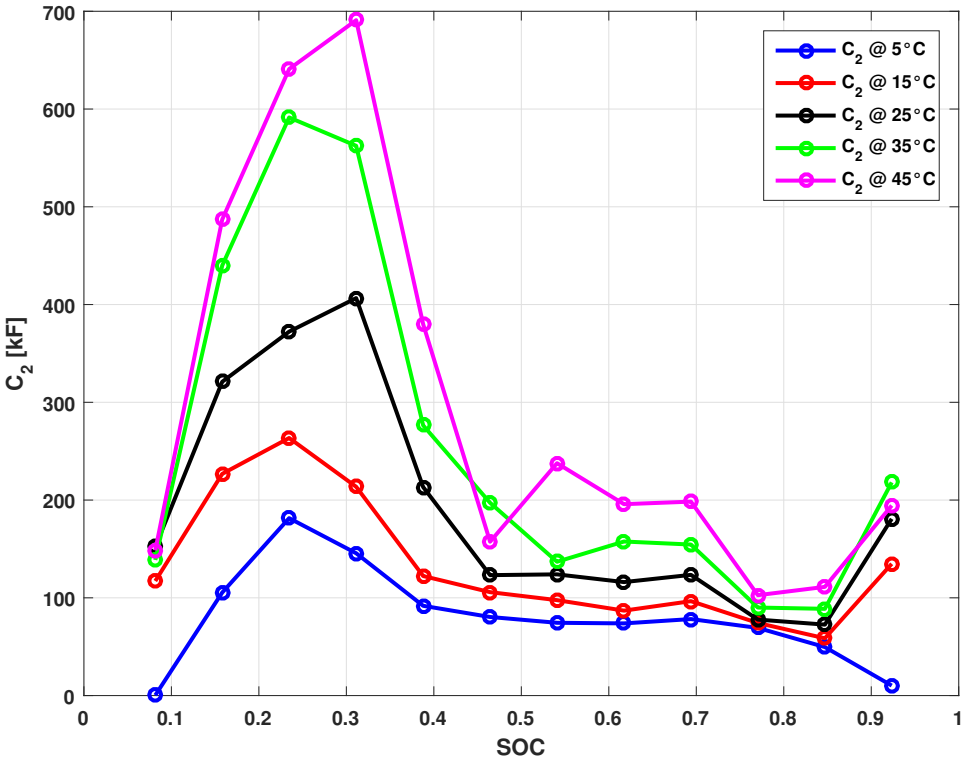


(b) C_1

Figure 5.7: Measured data showing the variation of the cell parameters R_1 and C_1 for different temperatures under 2C rate discharge pulse test.

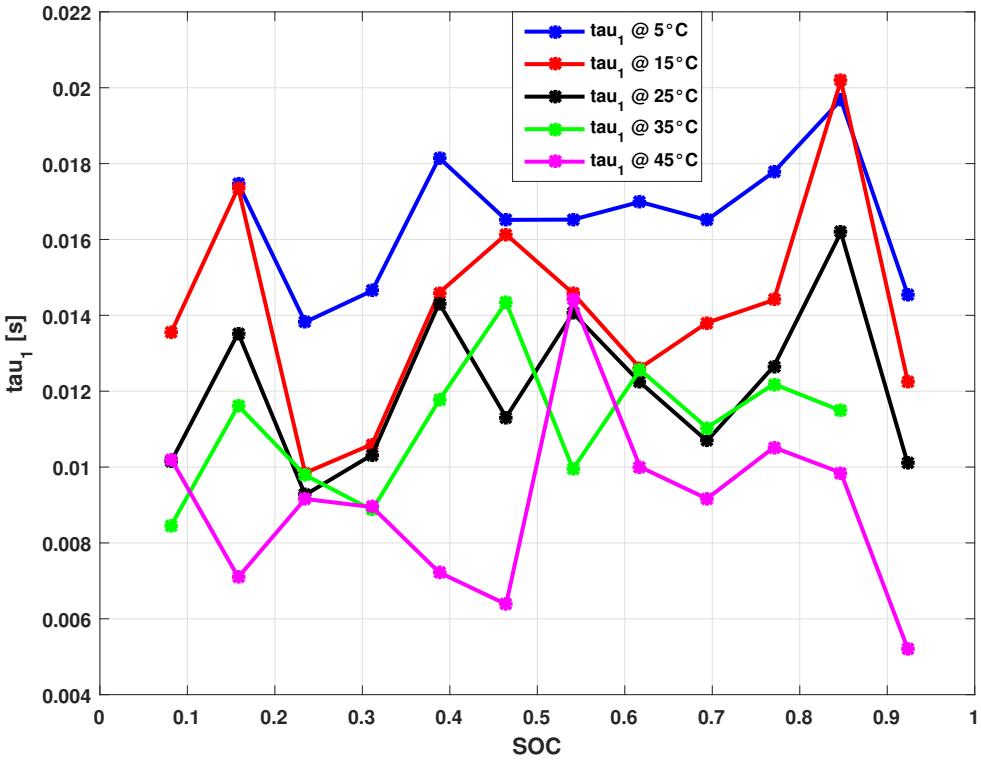


(a) R_2

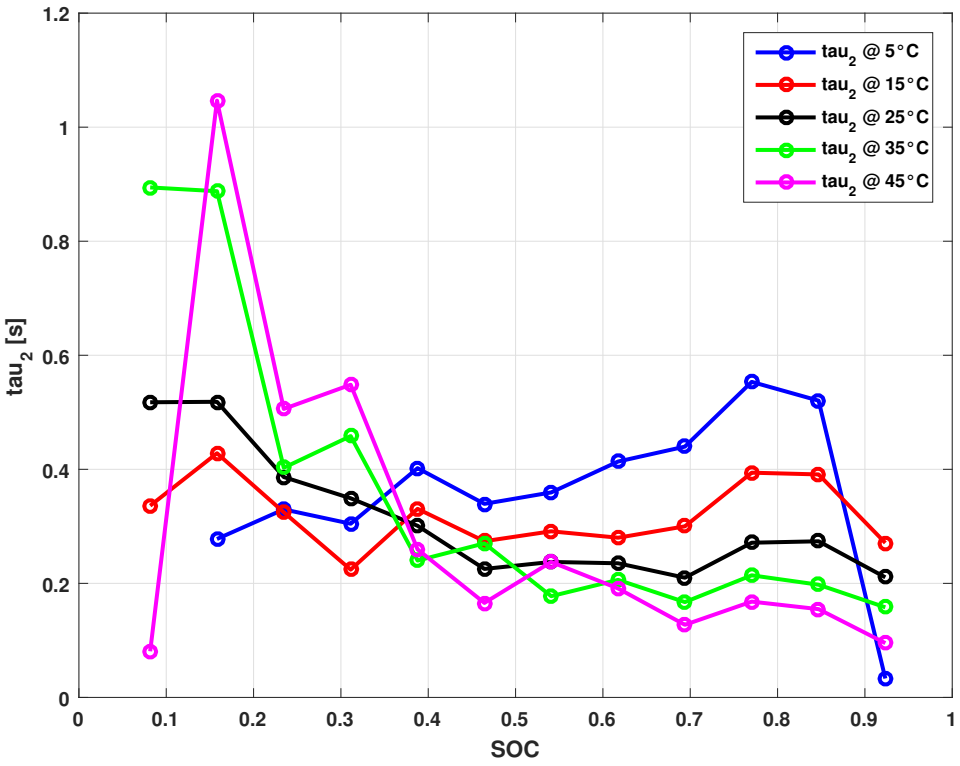


(b) C_2

Figure 5.8: Measured data showing the variation of the cell parameters R_2 and C_2 for different temperatures under 2C rate discharge pulse test.



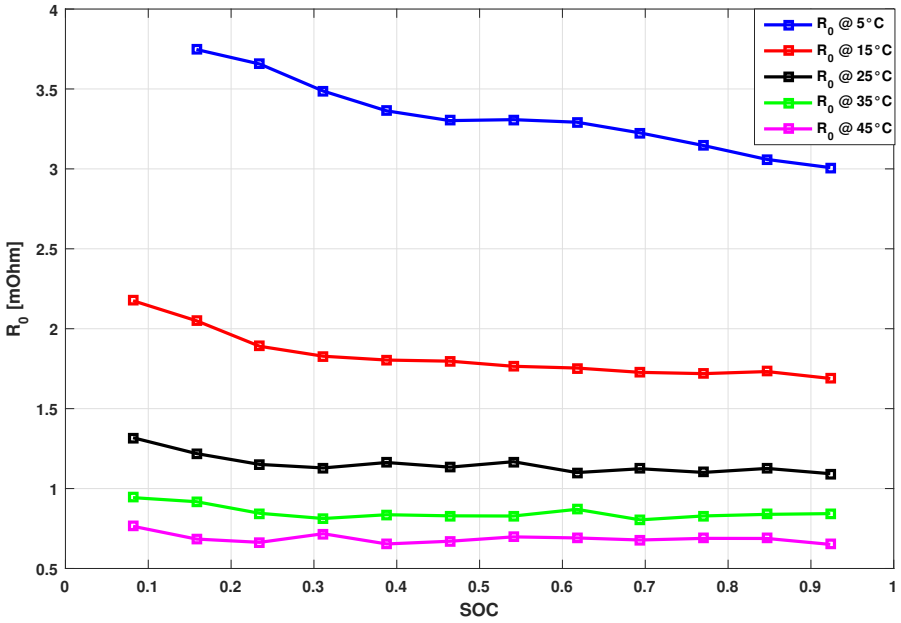
(a) τ_1



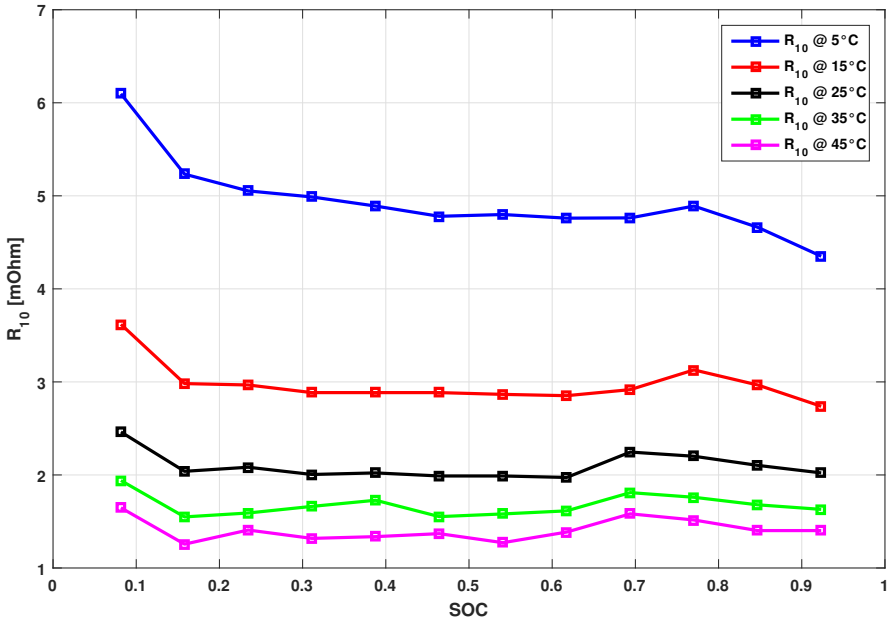
(b) τ_2

Figure 5.9: Measured data showing the variation of the time constants τ_1 and τ_2 for different temperatures under 2C rate discharge pulse test.

From Fig. 5.10, we don't observe much variation of the resistances R_0 and R_{10} with SOC, but we do observe similar variations with different temperatures as already discussed earlier.



(a) R_0



(b) R_{10}

Figure 5.10: Measured data showing the variation of the resistances R_0 and R_{10} for different temperatures under 2C rate discharge pulse test.

5.1.5 Verification of the entropic heat

As discussed in section 4.2.4, we conducted an experiment to approximate the specific heat of the cell and we used the same experiment settings to verify the existence of the entropic heat, but with loading the test cell rather than the dummy cell at 2 C-rate (20 A) current.

Firstly, the results for the thermal resistance of the leakage R_{th} and total heat capacity C_{th} from the specific heat experiment is 6.93 $\frac{K}{W}$ and 683.24 $\frac{J}{K}$ respectively. Taking the heat capacity of 2 charging wires with length of 0.6 m and diameter of 0.01 m for each and heat capacity of the aluminium cooling plate into account, the specific heat can be approximated as 1013 $\frac{J}{kg \cdot K}$ and this is the specific heat for a single cell only.

With the approximated thermal leakage of the insulation box and the temperature data of the 2C-rate (20 A) discharging test, we can approximate the dissipated power of the test cell during the discharging period and then compare it with the rate of joule heat, whether there is entropic heat can be clarified. And the rate of joule heat can be approximated by the product of the internal resistance and current squared, which in our case is obtained from the single cell electric model with 2 RC circuits. and the temperature input to the look-up of electric parameters is the temperature measured data of this test, so it's not related to the thermal model.

From Fig. 5.11, it is obvious that the total dissipated power of the cell is not equal to the rate of joule heat. Up to approximately 700 s the joule heat rate is greater than the total dissipated power, so in this time period the entropic heat is endothermic and after 700 s, the entropic heat is exothermic and adds up with the joule heat to increase the dissipated heat rate. In this way we have verified the existence of the entropic heat and also we can conclude that the entropic heat is reversible (i.e it can be both exothermic and endothermic) whereas the joule heat is irreversible (i.e it is exothermic) as discussed earlier in 2.3.4.

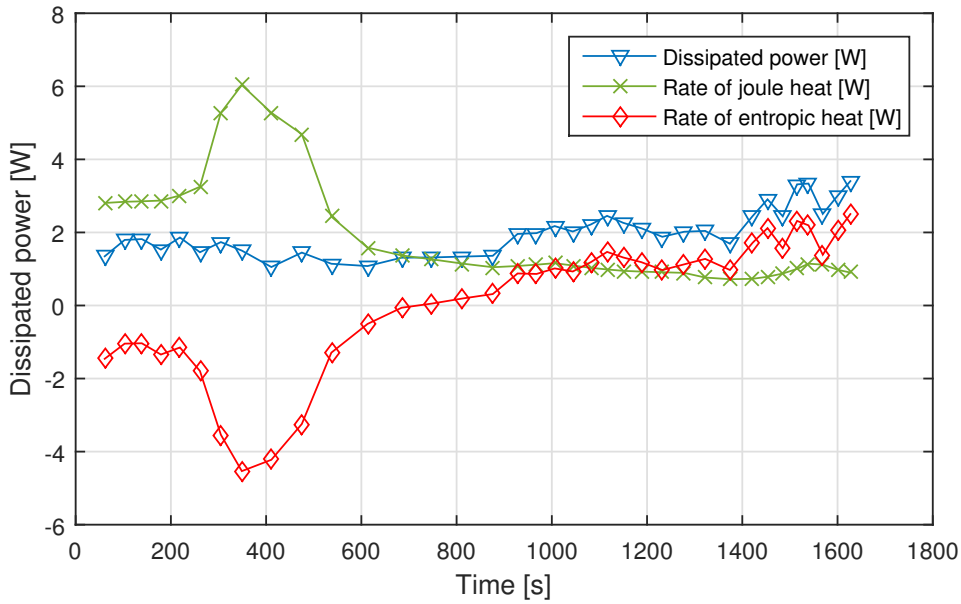


Figure 5.11: Comparison between the rate of joule heat and the total dissipated power of the cell at 23.9 $°C$ under 2C rate discharge current. The dissipated power is the measurement data and the rate of joule heat is the simulation data.

5.2 Sensitivity analysis of the battery pack thermal model

5.2.1 Contact pressure between the cell and the cooling plate

We have investigated the influence of contact pressure on the thermal behaviour between the cell and aluminium plate, for the cases where the lithium ion cell is located at the middle and at the side of the battery pack as shown in Fig. 3.3.

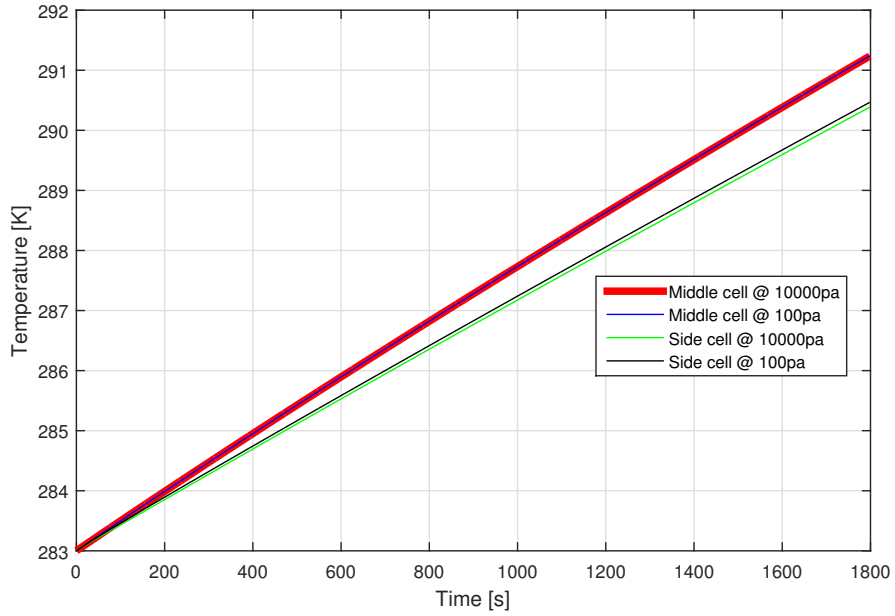


Figure 5.12: Simulated cell temperature data under different contact pressures for a 2C-rate discharging current.

We find that there is no obvious change in the thermal behavior when the contact pressure between the cell and aluminium cooling plate varies. We believe the reason is because in our model, each cell is releasing heat simultaneously with the same dissipated power.

This assumption is based on the fact that the active battery management system balances the cell charge in a multi-cell lithium ion battery pack to guard against damage and improve its lifetime [35]. If the temperature difference between the cells is minor, then the heat transfer mechanism between two cells through conduction is very small. We can also infer that, three orders difference of contact pressure doesn't cause three orders difference of the contact conductance between the two substances, which is shown in Table 5.1.

Table 5.1: Contact Conductance under different contact pressures

Contact conductance $W/(m^2 \cdot K)$	Thermal Grease	Contact pressure 100000 Pa	Contact pressure 100 Pa
Cell and polypropylene	No	8508.8	70.9
Cooling plate and polypropylene	Yes	148230	75849
Cell and cooling plate	Yes	234380	119930

5.2.2 Air gap between cell and cell

Influence of the air gap thickness on the thermal behaviour between two cells located at the middle and at the side of the battery pack have also been investigated. Feng [36] found that the thickness of the air gap is not negligible when stacking

five cells together without any package. However, in our model the results turn out to be the opposite.

The contact conductance between a cell and another cell without a cooling plate for 1 mm and 2 mm air gap is 0.963 and 0.929 $W/(m^2 \cdot K)$ respectively. From Fig. 5.13, it can be observed that there is no temperature difference when the air gap thickness is changed. This is because in our battery pack, there are aluminium cooling plates between a cell and another cell in some cases and the conductance between cell and aluminium cooling plate is shown in Table 5.1, which is much higher than the conductance between cell and cell with only air gap as mentioned in this paragraph, rather than the aluminium cooling plate. The heat generated from the cell flows easily through the aluminium cooling plate to the air inside the package, rather than flowing through the air gap to the other cells.

The only influence that a changing air gap will induce is an increase of the heat capacity and thermal mass of the air inside the package.

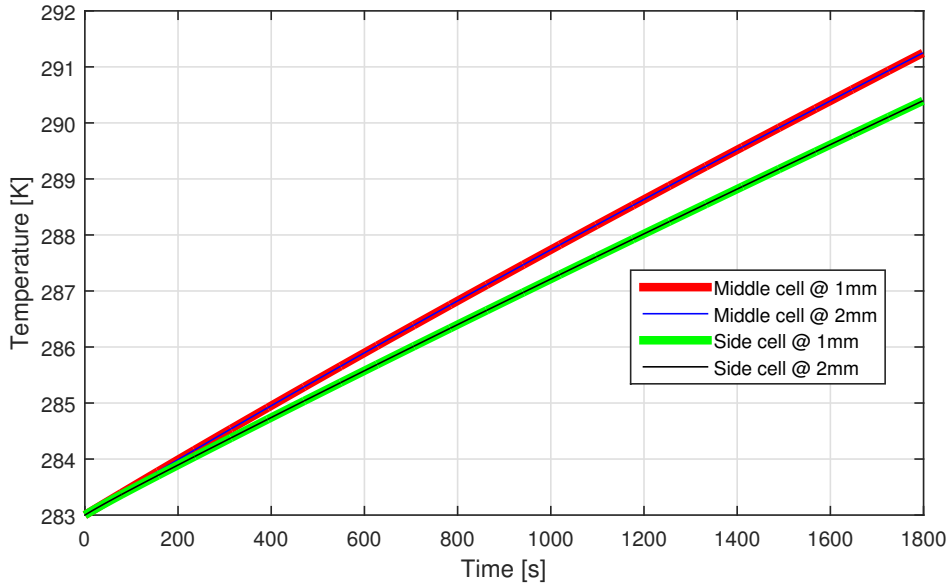


Figure 5.13: Simulated cell temperature data under different air gap thicknesses for a 2 C-rate discharge current

5.2.3 Volumetric velocity of cooling air

The heat generated from the cells is dissipated by the cooling air outside the battery package. So, it is worth seeing whether different volumetric velocities influence the battery pack thermal behavior.

As mentioned earlier, the forced convection coefficient is determined by the Reynolds number and the Prandtl number. When the volumetric velocity changes, the velocity of the cooling air also varies. In other words, the Reynolds number varies

corresponding to the volumetric velocity in our case. Specifically, when the volumetric velocity increases from 5 l/s to 10 l/s the forced convection coefficient rises 1.41 times as (3.6) and (3.3) show.

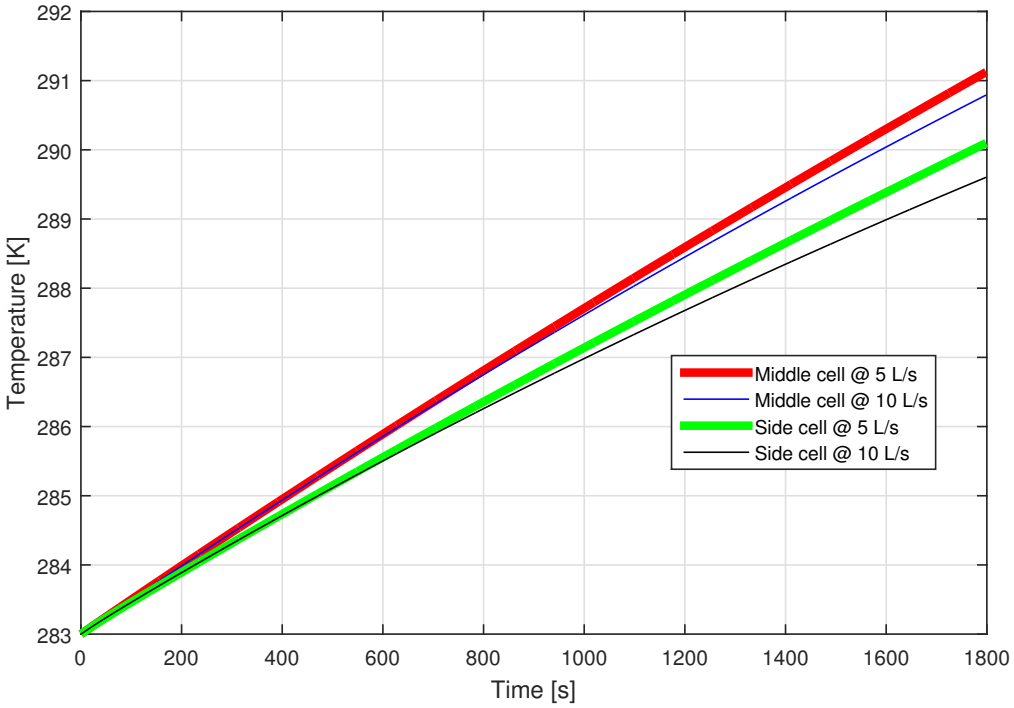


Figure 5.14: Simulated cell temperature data under different volumetric velocity of cooling air for a 2 C-rate discharge current

From Fig. 5.14, it is obvious that the volumetric velocity of cooling air has an influence on the thermal behavior of the lithium ion cells. And the reason is not only the change in the heat capacity of the cooling air, since the heat capacity is the product of the specific heat and the mass, variation of the volumetric velocity will induce the mass variation of the cooling air, but also the variation of the forced convection coefficient caused by variation of the Reynolds number.

5.2.4 Thermal time constant

In our model, the thermal calculation time interval and the time step of the flow circuit are both 0.1 s, which means that the flow solver calculates the convective heat transfer between the fluid (air flow) and the thermal masses every 0.1 s. Meanwhile, the thermal solver updates the thermal mass temperature based on the temperature of the previous step and the heat rate calculated by the flow solver in the previous time steps. Besides, the current profile of the driving cycle updates every 0.5 s, considering the thermal and fluid calculation time interval is 0.1 s that we have to do the interpolation for the current profile of the driving cycle. But for the loading current that we adopt for experiment, it's a continuous profile which we can take the current updating frequency as infinity high.

Usually, heat transfer takes time to develop and the rate of heat transfer can be characterized by the thermal time constant τ, as suggested in [8] according to

$$\tau = \frac{mC_p}{kA} \tag{5.1}$$

where m is the mass of the lithium cell, C_p is the specific heat of the cell, k is the heat transfer coefficient between two substances, and A is the cell surface area.

However, in our case the heat transfer mechanisms of different cell surfaces are different and can be divided into two parts which are shown Fig. 3.3; one way is that the heat is transferred by conduction between the cells and the polypropylene package, then transferred to the air outside the package by free convection, while another way is that the heat transferred by free convection between the cells and the air inside the polypropylene package and then by conduction through the polypropylene package to be ultimately transferred to the air outside the package by free convection.

$$\tau = \frac{mC_p}{k_1A_1 + k_2A_2} \tag{5.2}$$

where, k_1 and k_2 are the heat transfer coefficients for the combination of conduction and convection in our case , A_1 and A_2 are the corresponding heat transfer surface areas, which is 0.1276 and 0.1038 m^2 respectively

$$k_1 = \frac{1}{\frac{1}{h_1} + \frac{\delta_1}{\lambda_1} + \frac{1}{h_1} + \frac{\delta_2}{\lambda_2} + \frac{1}{h_2}} = 0.44677\frac{W}{m^2K} \tag{5.3}$$

$$k_2 = \frac{1}{\frac{\delta_2}{\lambda_2} + \frac{\delta_3}{\lambda_3} + \frac{1}{h_2}} = 12.5\frac{W}{m^2K} \tag{5.4}$$

where h_1 is the convection coefficient between cell and the air inside the package, δ_1 is the thickness of the air inside the package, λ_1 is the conductivity of the air inside the package, δ_2 is the thickness of the plastic package, λ_2 is the conductivity of the package material(polypropylene), h_2 is the convection coefficient between the package and the air outside the package, δ_3 the characteristic height of the cell and λ_3 is the cell conductivity of the cell along the plane direction.

Using (5.2),(5.3) and (5.4), the time constant of our system turns out to be 3528 s, which means that after the loading case, the temperature difference between the cell and the cooling air outside the battery package as $T - T_\infty$ takes 3528 s to decay to $\frac{1}{e}$ of the initial $T_0 - T_\infty$ (T_0 means the cell temperature at the end of the loading case), as:

$$\frac{T - T_\infty}{T_0 - T_\infty} = \frac{1}{e} \tag{5.5}$$

5.3 Comparison between the experiment and the simulation results

5.3.1 Terminal voltage comparison between the simulation prediction and the experiment

Fig. 5.15 shows the comparison of the battery pack terminal voltage between the simulation and the experiment under 2C ($20A$) discharging starting from 89 % SOC to 2 % SOC at 10 $°C$. We can observe that during the discharge period, the simulation result turns out to be a bit higher than the experiment values and this is because without a suitable RC circuit, the voltage drop due to the RC circuit is not taken into account. So the terminal voltage in the simulation result turns out to be a bit higher than the experiment result.

During the relaxation period (when no current flows) starting from around 1500 s, the simulation result shows a steep jump, whereas the experiment result shows a gradual rise. This is because in the simulation model we have neglected the RC circuit, which explains why the dynamic behavior has not been captured.

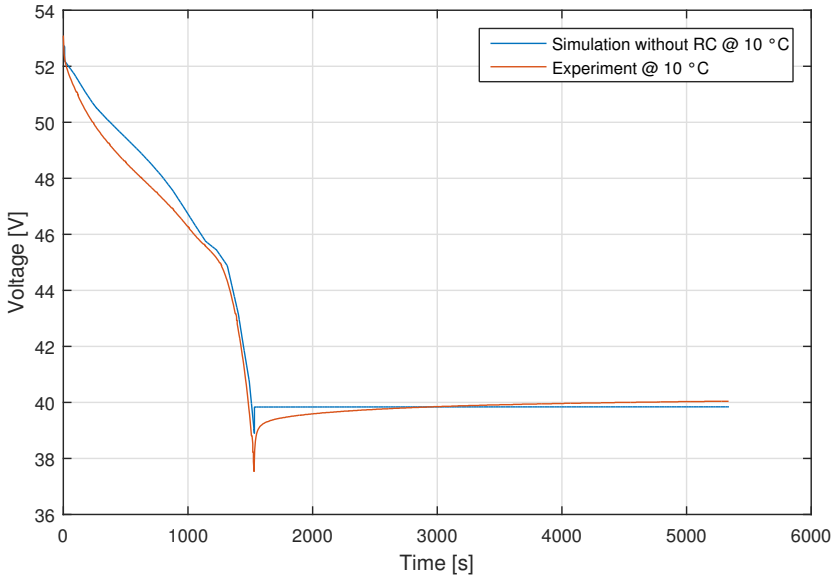


Figure 5.15: Terminal voltage comparison between measurement and 0 RC circuit model at 10 $°C$ under 2C rate discharge current, discharging the battery pack from 89 % SOC to 2 % SOC.

Fig. 5.16 shows the simulation result with 2 RC circuits and we can see that the terminal voltage estimation fits much better with the experiment result than without any RC block. At the end of the rest phase there is a difference between the measured OCV and the simulated OCV. This is because in our simulation model we made an assumption that each cell has the same capacity, which is not the case in reality where the SOC estimation is not very precise because different cells have different

capacities.

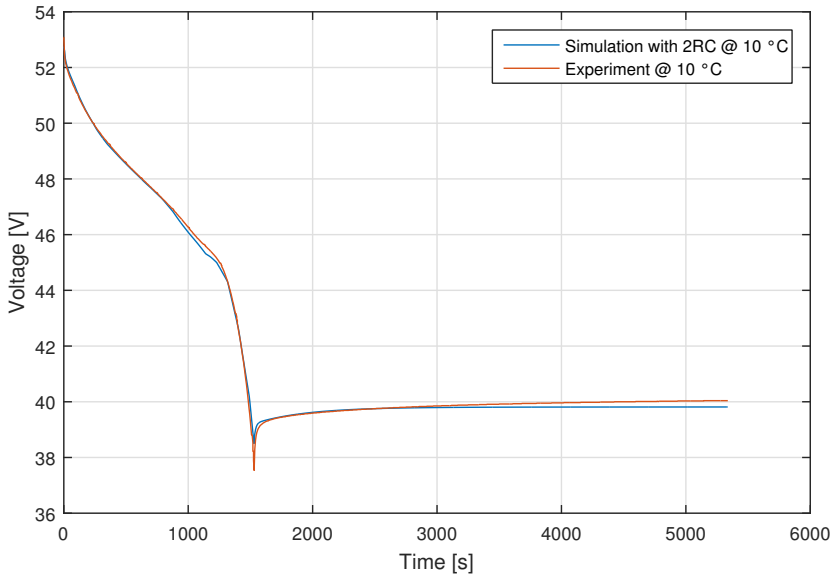


Figure 5.16: Terminal voltage comparison between the measurement and the 2 RC circuits model at 10 $°C$ under 2C rate discharge current, discharging the battery pack from 89 % SOC to 2 % SOC.

Fig. 5.17 shows the comparison of the terminal voltage between the simulation and the experiment under 2C rate ($20A$) discharge current, starting from 89 % SOC to 2 % SOC at 35 $°C$. We can see that the simulation result fits the experiment quite well. If we compare Fig. 5.15 and Fig. 5.17, we can see that during the discharge phase at 10 $°C$, the simulation result of the terminal voltage is a bit higher than the experiment result. As the temperature increases to 35 $°C$ the resistance of the cells decrease, so the voltage drop decreases than at 10 $°C$.

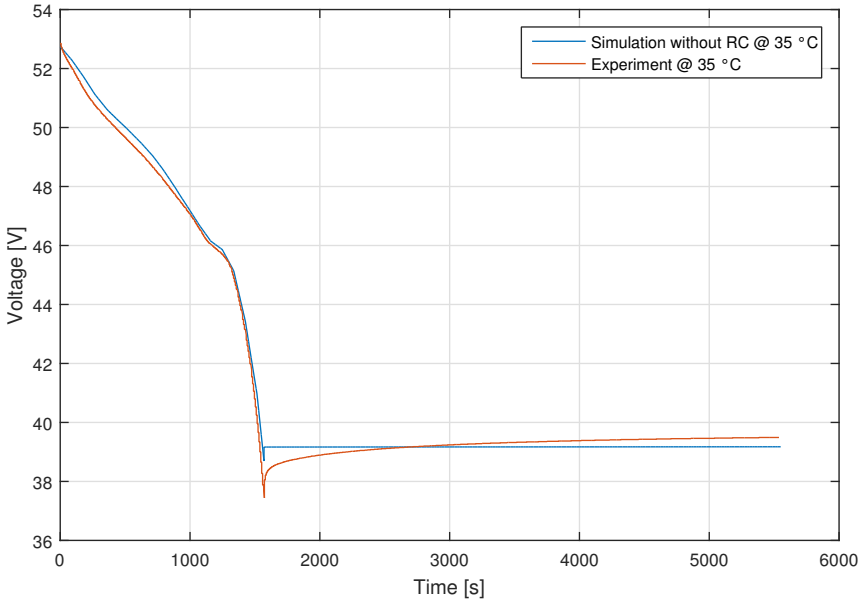


Figure 5.17: Terminal voltage comparison between the measurement and the 0RC circuit model at 35 $°C$ under 2C rate discharge current, discharging the battery pack from 89 % SOC to 2 % SOC.

From Fig. 5.18, we can see the simulation result with the 2RC circuit model and the experiment result at 35 $°C$. It seems that with the 2RC circuit model the simulation curve fits the experiment curve better, but it's necessary to mention that with the 0RC circuit model, the CPU time for the simulation is around 4 minutes, while with 2RC models, the CPU time for the simulations exceeds 20 minutes. The user should find a balance between the accuracy of simulation and computation time according to the requirements.

Comparing the simulation and experiment results for 10 $°C$ and 35 $°C$, we can see that the RC circuit plays an important role under low temperature because the internal resistance of the cell is temperature-dependent. At low temperature, the internal resistance is higher as shown in Fig. 5.7 and Fig. 5.8, so the voltage drop on the internal resistance is larger than at a higher temperature and the offset between the simulation and experiment data is easily captured.

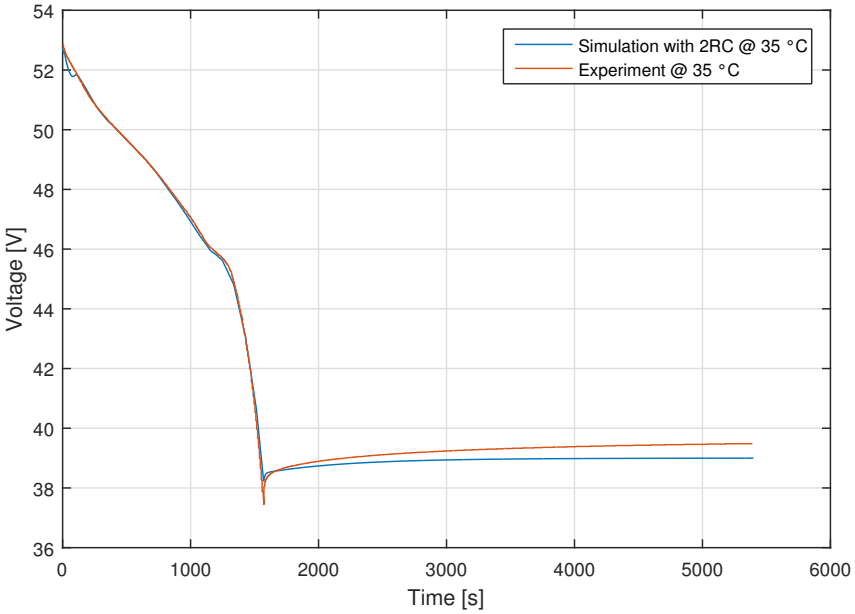


Figure 5.18: Terminal voltage comparison between the measurement and the 2 RC circuit model at 35 $°C$ under 2C rate discharge current, discharging the battery pack from 89 % SOC to 2 % SOC.

Actually we have done another loading case as a square waveform with 2C (20 A) current under 25 $°C$ and the SOC varies within 39 % and 59 %. And the simulation result from the model which includes 2 RC models fits the experiment result well for this loading case.

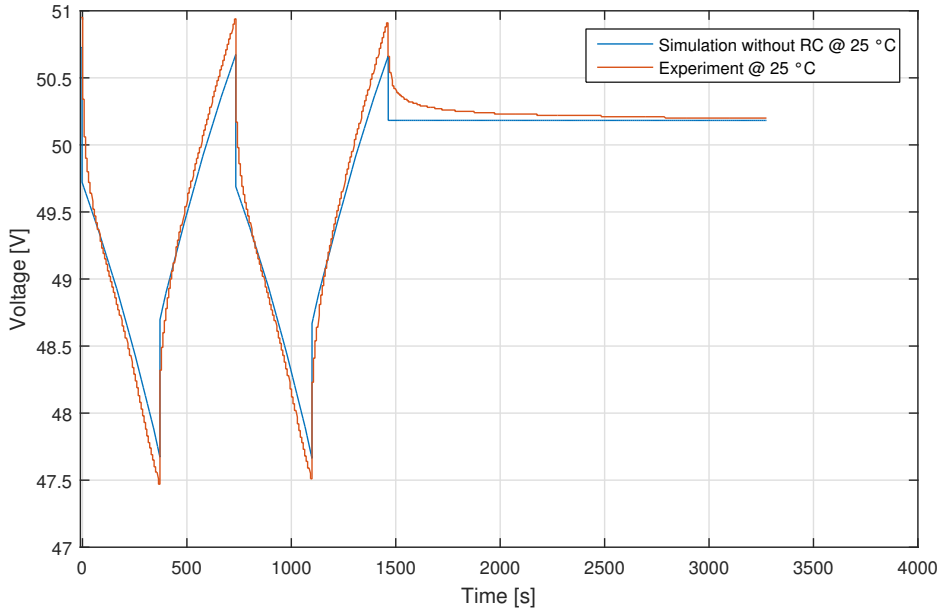


Figure 5.19: Terminal voltage comparison between measurement and 0 RC circuit model at 25 °C under 2C rate charge discharge current, with SOC varying within 39 % to 59 %.

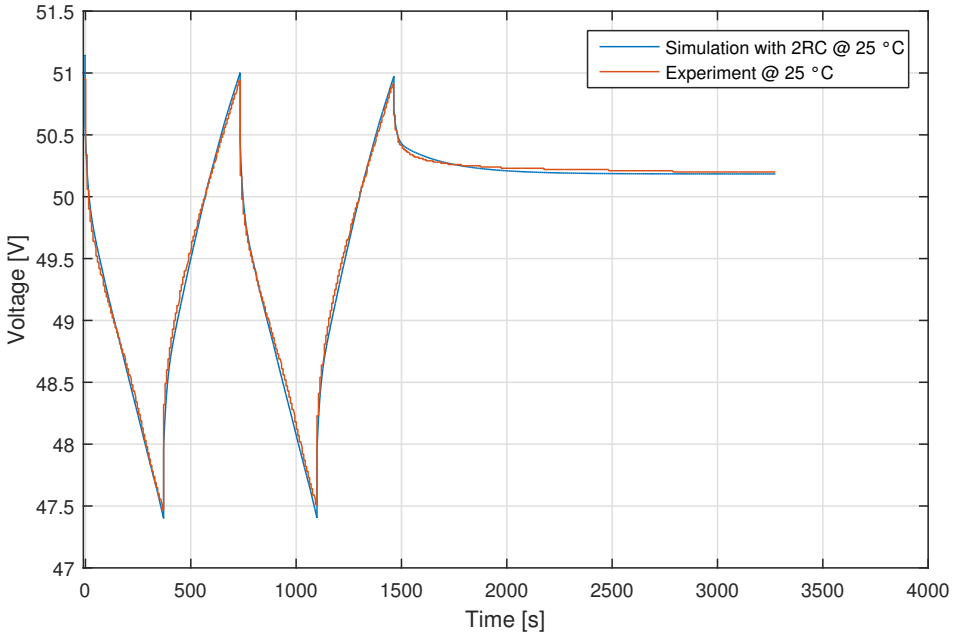


Figure 5.20: Terminal voltage comparison between measurement and 2 RC circuits model at 25 °C under 2C rate charge discharge current, with SOC varying within 39 % to 59 %.

5.3.2 Temperature comparison between the simulation model and the experiment

Fig. 5.21 shows the comparison between the simulation and the experiment measurement data. Here, we have adopted the R_{10} resistance look up to the simulation model without two RC circuits and we found that the error of the temperature prediction is much higher than when we include the two RC circuits into the model.

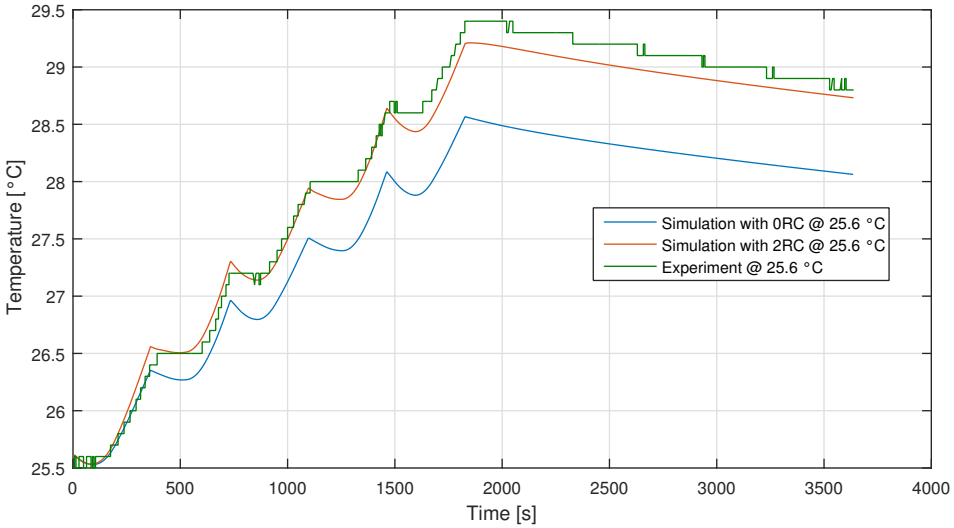


Figure 5.21: Temperature comparison at 25 $°C$ under 2C rate charge-discharge current, with the SOC varying between 39 % SOC to 59 % SOC.

Fig. 5.22 shows the difference between the experiment temperature data and the simulation data with two RC and without RC networks. We can observe that the error for the model without the RC links can reach 3.2 %, while the error for the model with 2 RC links is only 1.5 %. This is because the R_{10} resistance is only representable when the charging or discharging pulse is shorter than 10 s and for this loading case, the charging and discharging pulse reaches 360 s. As observed in 5.3.1, with 2 RC models, the prediction of the terminal voltage from the simulation model is much better than without RC model as well. The reason for employing R_{10} is because this is the value, we can probably get from the supplier.

It is worth mentioning that 2 RC circuit models can provide us with much higher precision, but it will lead to an increase in the CPU computation time. From our observations, we have noted that the battery pack electro-thermal model without any RC circuit takes around 2 minutes computation time, whereas the same model fitted with two RC circuits takes approximately 8 minutes.

Fig. 5.23 shows the pack temperature comparison between the simulation model with 2 RC links and the experiment result and since they match each other well, it can be proved that the thermal boundary conditions of the battery pack are closer to reality.

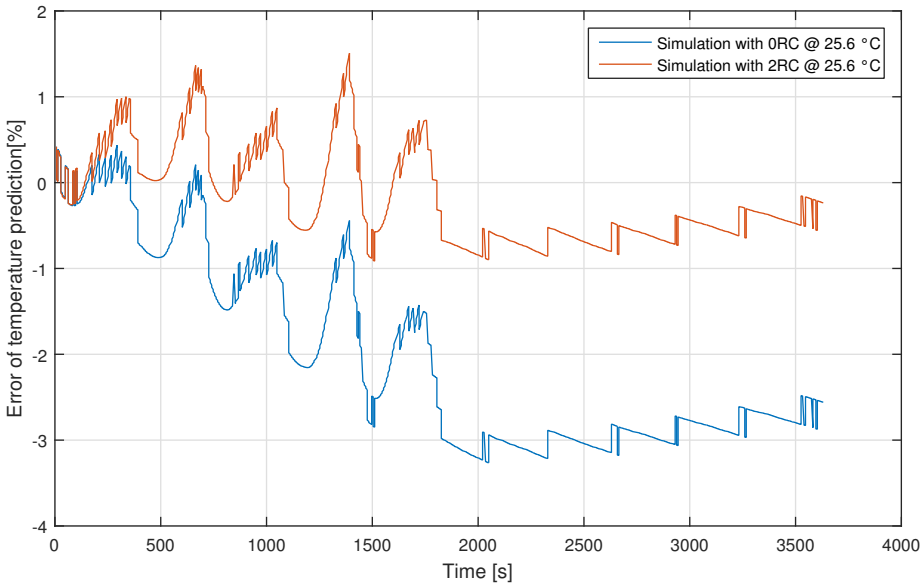


Figure 5.22: Error of the temperature prediction at 25.6 °C under 2C rate charge-discharge current, with SOC varying between 39 % to 59 %. The temperature difference between the simulation models and the experiment as shown in Fig. 5.21 has been plotted here.

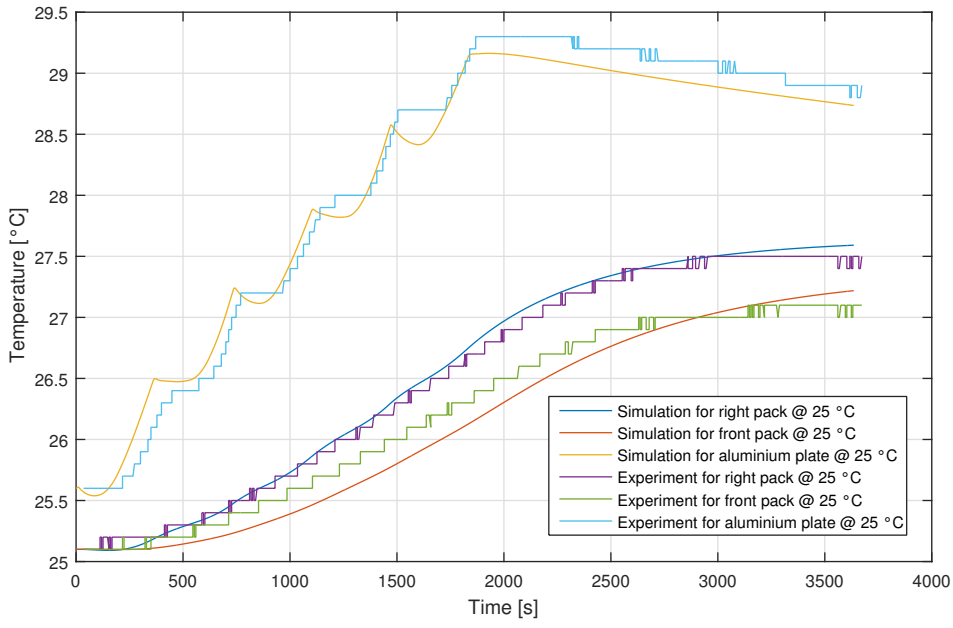


Figure 5.23: Battery pack temperature comparison between the measured experiment data and the 2 RC circuit simulation model data at 25 °C under 2C rate charge discharge current, with SOC varying between 39 % to 59 %.

As discussed earlier in section 5.1.5, where we have verified the existence of entropic heat, it is interesting to see its role in the temperature prediction. We run the

simulation of the charging-discharging load case at 25 $°C$ under 2C rate again but this time without taking the entropic heat into account.

Fig. 5.24 and Fig. 5.25 shows the comparison between the simulation and the experiment without the entropic heat and an error analysis respectively. We can see that the temperature behavior for Fig. 5.24 is quite different from Fig. 5.21, as the dynamic behavior is not captured in the former result. As for the error analysis, the maximum error for the whole simulation duration is almost the same, but we should notice that when we don't take the entropic heat into account, we will miss the important thermal dynamic behaviors.

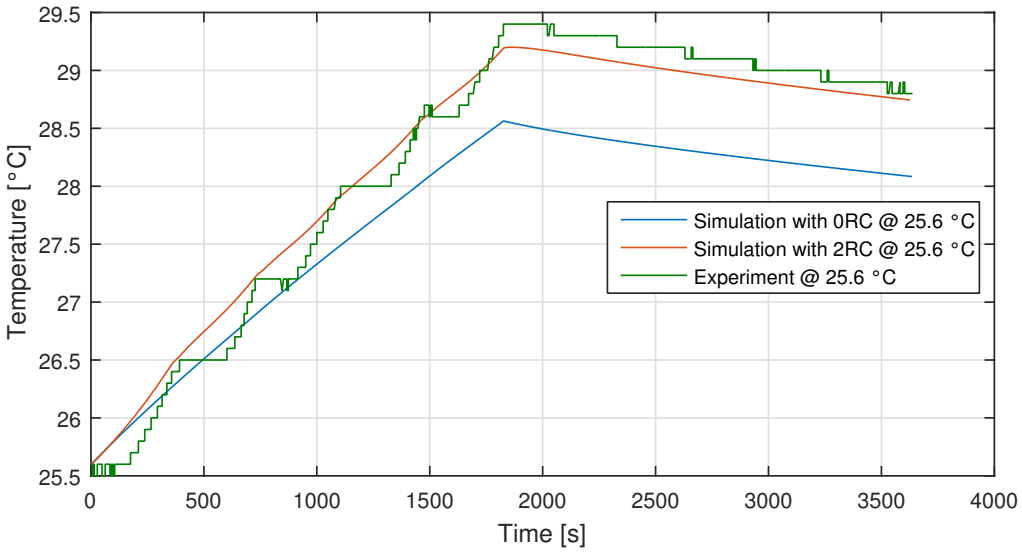


Figure 5.24: Temperature comparison at 25 $°C$ without the entropic heat under 2C rate charge discharge current, with SOC varying between 39 % to 59 %. A comparison with Fig. 5.21 reveals the omission of thermal dynamic behavior here.

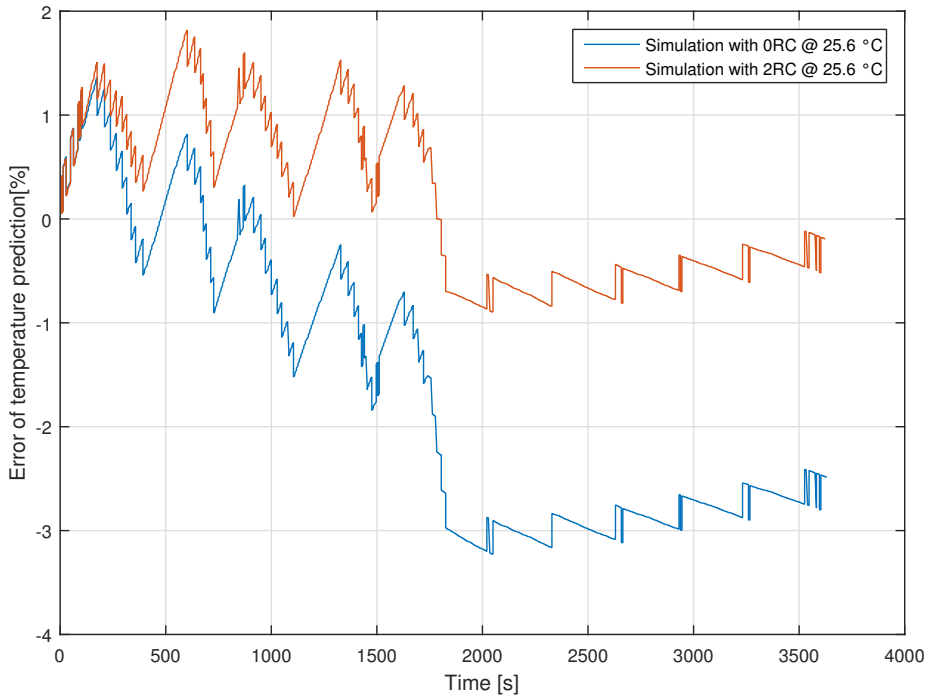


Figure 5.25: Error of the temperature prediction at 25 $°C$ without entropic heat into account under 2C rate charge discharge current, with SOC varying within 39 % to 59 %.

5.4 Simulation with the WLTP driving cycle

Finally, we load the battery simulation model with one WLTP driving cycle and obtain the temperature distribution as shown in Fig. 5.26. The main aim is to show the role that the entropic heat plays at the WLTP driving cycle level. Also, the initial SOC for the battery pack was set to be at 50 %, which was decided by us for the simulation.

We can observe that the entropic heat is exothermic (i.e it combines with the joule heat to contribute tot the total heat) from 0 s to approximately 800 s and is endothermic (i.e it offsets the joule heat) from approximately 800 s to the end of the WLTP driving cycle. Although the temperature trend is quite similar, the magnitude is different for most time durations, and the temperature difference between the simulations when we consider and when we don't take the entropic heat into account has been shown in Fig. 5.28. This shows that it maybe necessary to take the entropic heat into account.

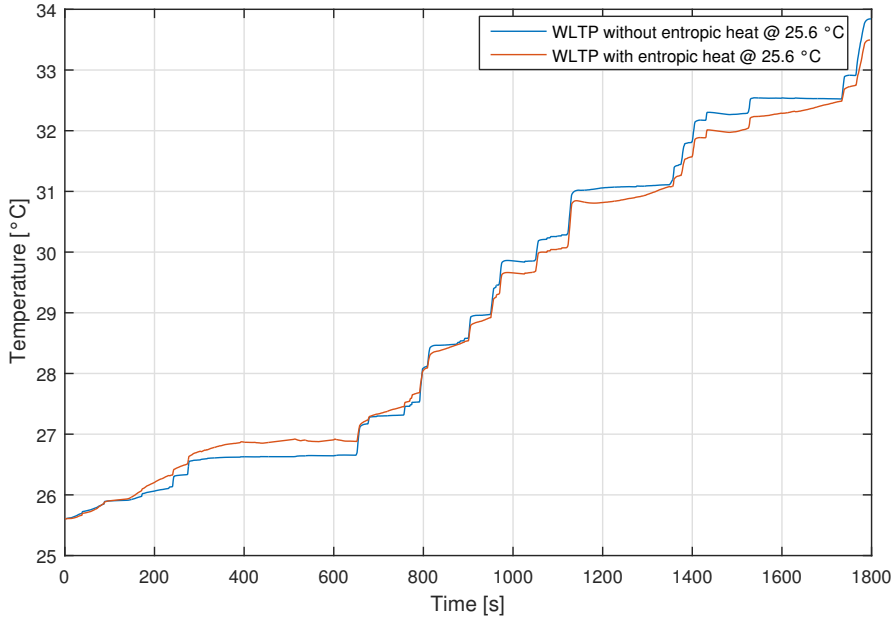


Figure 5.26: Simulated temperature comparison with the WLTP driving cycle on the entropic heat at 25.6 $°C$.

Fig 5.27 presents the variation of SOC with the WLTP driving cycle. A comparison with Fig. 5.5 shows that the entropic heat coefficient has a negative sign upto approximately 45 % SOC and thereafter it changes its sign. In Fig. 5.27 upto 800 seconds or less than 45 % SOC, the entropic heat is exothermic (so, the entropic heat aids the joule heat) and then it becomes endothermic (so, the entropic heat offsets the joule heat) from 800 s till the end of the WLTP driving cycle.

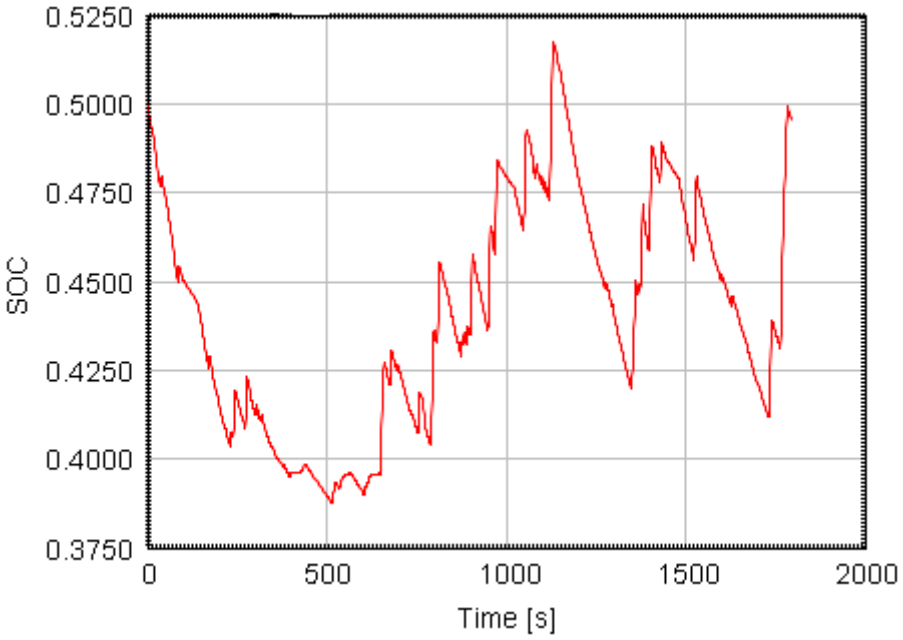


Figure 5.27: Simulated SOC variation with the WLTP driving cycle.

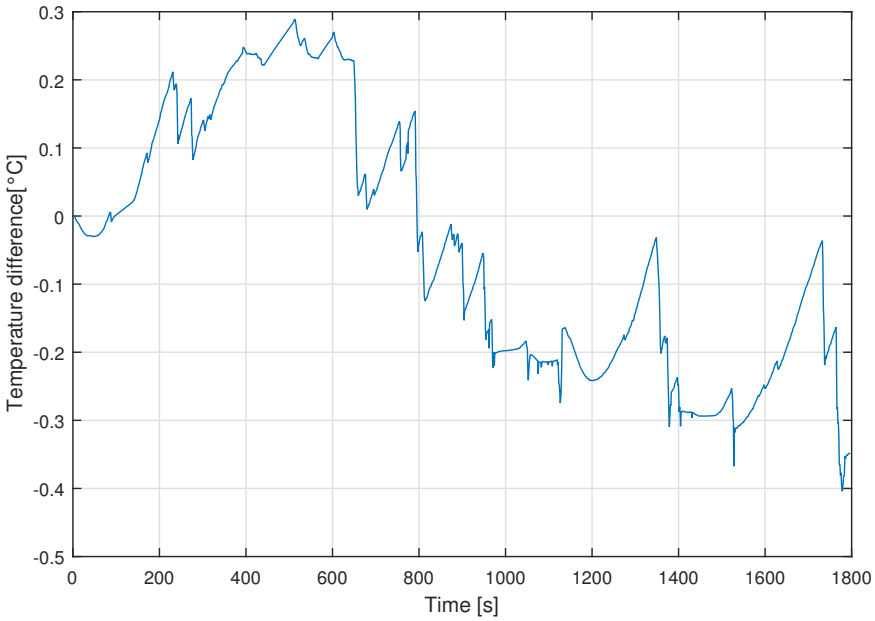


Figure 5.28: Temperature difference with WLTP driving cycle on the entropic heat factor.

6
Conclusions

In this chapter we have come up with our thoughts and the ideas which we both have shared and learned from each other and from the project as a whole.

6.1 Conclusions

The thesis work has established an electro-thermo battery model to predict the terminal voltage, SOC and temperature of the battery under certain loading cases and compare the simulation results with the measurement data, the error is less than 4 % for the temperature prediction.

As for the prediction of the voltage on the battery during loading period, we find that adopting 2 RC links has a higher precision than without any RC link, which also enables us to capture the dynamic electrical behavior and increase the precision of temperature prediction as well.

As for the thermal sensitivity analysis of the battery pack model, when the battery pack is well sealed which means there is no air exchange between the battery pack and the ambient, the influence of the air gap and the contact pressure between the cell and another cell or between the cell and the aluminium cooling plate is minor. Only the volumetric velocity of the cooling air surrounding the battery pack has a major influence on the battery pack thermal behavior.

Through the experiment, we have not only verified that the entropic heat can be either exothermic or endothermic, but also managed to quantify the entropic heat coefficient and it can be concluded that entropic heat plays an important role together with the joule heat. Crucial thermal dynamic behaviour is lost, when we neglect the entropic heat.

6.2 Discussions

The findings about the entropic heat can be adopted in the design of the control strategy of hybrid vehicles, specifically, during the coupling of the alternator and internal combustion engine, we can control the load on the alternator to realize the control of the current on the battery, to enable the entropic heat offset the joule heat and decrease the temperature of the battery without imposing new cooling solutions, thereby reducing the cost.

Table 6.1 shows how the entropic heat could affect the thermal behavior of the NMC chemistry battery pack.

Table 6.1: Effect of the entropic heat on the thermal behavior for NMC chemistry battery pack

SOC	Entropic heat coefficient	Current	Entropic Heat
<45%	-	-(discharge)	endothermic
	-	+(charge)	exothermic
>45%	+	-(discharge)	exothermic
	+	+(charge)	endothermic

6.3 Future work

In the electrical model, certain interesting observations for example, a peculiar resistance behavior from approximately 70 % to 90 % SOC, randomness in the capacitance behavior could not be explained. We believe that research in the battery chemistry aspects could hold solutions to such phenomena.

In the thermal model, for the determination of the convection coefficient, we need to deal with the dimensionless numbers, such as the Grashof Number and Nusselt Number because in our thesis we have adopted empirical equations for approximation. We reckon that if more calibration tests can be done for the approximation of the dimensionless numbers, the accuracy and precision of the temperature prediction can be even higher. Moreover SOC control can also be implemented as we have seen in section 5.4.

It would be worth implementing the model verification for the WLTP driving cycle. In this thesis, we have only verified the battery model with a square current waveform but we are still not sure about the robustness of our battery model in real time usage case. As long as the verification on the driving cycle is done, a further step can be validation test by online tests on the vehicle.

Bibliography

[1] Xiao, H. "Battery Thermal Management in Electric Vehicles." Ansys Inc., Canonsburg (2010).

[2] Linden, David, and T. B. Reddy. "Handbook of Batteries, 2002." 1e42: 4.

[3] Pesaran, Ahmad A. "Battery thermal management in EV and HEVs: issues and solutions." Battery Man 43.5 (2001): 34-49.

[4] Pesaran, Ahmad, et al. "Tools for designing thermal management of batteries in electric drive vehicles." Large Lithium Ion Battery Technology and Application Symposia Advanced Automotive Battery Conference Pasadena. 2013.

[5] Doughty, Dan, and E. Peter Roth. "A general discussion of Li ion battery safety." Electrochemical Society Interface 21.2 (2012): 37-44.

[6] Pesaran, Ahmad, Shriram Santhanagopalan, and G. Kim. "Addressing the impact of temperature extremes on large format Li-Ion batteries for vehicle applications." National Renewable Energy Laboratory (2013).

[7] `http://web.mit.edu/evt/summary_powertrains.pdf`.

[8] Incropera, Frank, and David DeWitt. "Introduction to heat transfer." (1985).

[9] Team, MIT Electrical Vehicle "A Guide to Understanding Battery Specifications" (2008).

[10] Lee, Jin-Fa, Robert Lee, and Andreas Cangellaris. "Time-domain finite-element methods." IEEE transactions on antennas and propagation 45.3 (1997): 430-442.

[11] Uddin, Ahmed Imtiaz, and Jerry Ku. "Design and Simulation of Lithium-Ion Battery Thermal Management System for Mild Hybrid Vehicle Application." No. 2015-01-1230. SAE Technical Paper, 2015.

[12] Zhang, S. S., K. Xu, and T. R. Jow. "The low temperature performance of Li-ion batteries." Journal of Power Sources 115.1 (2003): 137-140.

[13] Bernardi, D., E. Pawlikowski, and John Newman. "A general energy balance for battery systems." Journal of the electrochemical society 132.1 (1985): 5-12.

[14] Newman, John, and Karen E. Thomas-Alyea. Electrochemical systems. John Wiley and Sons, 2012.

[15] Thomas, Karen E., John Newman, and Robert M. Darling. "Mathematical modeling of lithium batteries." Advances in lithium-ion batteries. Springer US, 2002. 345-392.

[16] Ma, Yue, Ho Teng, and Marina Thelliez. "Electro-thermal modeling of a lithium-ion battery system." SAE International Journal of Engines 3.2010-01-2204 (2010): 306-317.

[17] `https://gigaom.com/2011/03/18/the-three-laws-of-batteries/-and-a-bonus-zeroth-law/`

[18] Dinger, Andreas, et al. “Batteries for electric cars: Challenges, opportunities, and the outlook to 2020.” Boston Consulting Group (2010).

[19] Saft . “Lithium-ion battery life” Saft (2014).

[20] Anderson, D. “Status and trends in the HEV/PHEV/EV battery industry.” Rocky Mountain Institute (2008).

[21] http://energyskeptic.com/2015/electric-vehicle-overview/

[22] https://www6.slac.stanford.edu/news/2015-06-17-study-finds-way/-prevent-fires-next-generation/-lithium-batteries.aspx

[23] http://www.idtechex.com/research/articles/48v-vehicle-systems-becoming-significant-00008266.asp

[24] Viswanathan, Vilayanur V., et al. “Effect of entropy change of lithium intercalation in cathodes and anodes on Li-ion battery thermal management.” Journal of Power Sources 195.11 (2010): 3720-3729.

[25] http://batteryuniversity.com/learn/article/types_of_battery_cells

[26] Pillot, C. “Battery market development for consumer electronics, automotive, and industrial: materials requirements and trends.” The 11th China International Battery Fair, ShenZhen, China (2014).

[27] Department 98140, Volvo Cars Group.

[28] Yang Shiming, and Tao Wenxuan. “Heat Transfer” (2006).

[29] Yovanovich, M. M., J. R. Culham, and P. Teertstra. “Calculating interface resistance.” Electronics Cooling 3.2 (1997): 24-29.

[30] Antonetti, VINCENT W., and M. M. Yovanovich. “Thermal contact resistance in microelectronic equipment[at physical junctions].” International Journal for Hybrid Microelectronics 7.3 (1984): 44-50.

[31] Cooper, M. G., B. B. Mikic, and M. M. Yovanovich. “Thermal contact conductance.” International Journal of heat and mass transfer 12.3 (1969): 279-300.

[32] Antonetti, V. W., T. D. Whittle, and R. E. Simons. “An approximate thermal contact conductance correlation.” Journal of Electronic Packaging 115.1 (1993): 131-134.

[33] Yovanovich, M. “New Contact and Gap Correlations for Confroming Rough Surfaces.” AIAA 16th Thermophysics Conference. 1981.

[34] GB/T 14234-93

[35] Bonfiglio, Carl, and Werner Roessler. “A cost optimized battery management system with active cell balancing for lithium ion battery stacks.” Vehicle Power and Propulsion Conference, 2009. VPPC’09. IEEE. IEEE, 2009.

[36] Feng Xuning, et al. “Experiments and modeling of anisotropic thermal conductivity of lithium-ion batteries.” J Automotive Safety and Energy, 3.2 (2012): 158-164.

[37] Huria, Tarun, et al. “High fidelity electrical model with thermal dependence for characterization and simulation of high power lithium battery cells.” Electric Vehicle Conference (IEVC), 2012 IEEE International. IEEE, 2012.

[38] Ji, Yan, Yancheng Zhang, and Chao-Yang Wang. “Li-ion cell operation at low temperatures.” Journal of The Electrochemical Society 160.4 (2013): A636-A649.

[39] Electric Power Engineering, Chalmers University of Technology.

[40] Department 94250, Volvo Cars Group.

[41] http://www.engineeringtoolbox.com/specific-heat-metals-d_152.html
[42] https://gigaom.com/2011/06/29/why-lithium-ion-batteries-die-so-young/7/
[43] https://areweanycloser.wordpress.com/2013/06/21/dendritic-lithium-and-battery-fires/